



OPEN

## Quantum mechanics insights into melatonin and analogs binding to melatonin MT<sub>1</sub> and MT<sub>2</sub> receptors

Gabriela de Lima Menezes<sup>1,2</sup>, Katyanna Sales Bezerra<sup>1,4</sup>, Jonas Ivan Nobre Oliveira<sup>1</sup>, John Fontenele Araújo<sup>3</sup>, Douglas Soares Galvão<sup>4</sup>, Roosevelt Alves da Silva<sup>5</sup>, Marielena Vogel Saivish<sup>6,7</sup> & Umberto Laino Fulco<sup>1,2</sup>✉

Melatonin receptors MT<sub>1</sub> and MT<sub>2</sub> are G protein-coupled receptors that mediate the effects of melatonin, a hormone involved in circadian rhythms and other physiological functions. Understanding the molecular interactions between these receptors and their ligands is crucial for developing novel therapeutic agents. In this study, we used molecular docking, molecular dynamics simulations, and quantum mechanics calculation to investigate the binding modes and affinities of three ligands: melatonin (MLT), ramelteon (RMT), and 2-phenylmelatonin (2-PMT) with both receptors. Based on the results, we identified key amino acids that contributed to the receptor-ligand interactions, such as Gln181/194, Phe179/192, and Asn162/175, which are conserved in both receptors. Additionally, we described new meaningful interactions with Gly108/Gly121, Val111/Val124, and Val191/Val204. Our results provide insights into receptor-ligand recognition's structural and energetic determinants and suggest potential strategies for designing more optimized molecules. This study enhances our understanding of receptor-ligand interactions and offers implications for future drug development.

Melatonin (N-acetyl-5-methoxytryptamine) is a neurohormone secreted during sleep that was first isolated from melanocytes of frogs and fish by Lerner et al.<sup>1,2</sup> In 1993, it was discovered that melatonin is secreted by the pineal gland of all vertebrates and is involved in regulating circadian rhythms<sup>3</sup>. The secretion of melatonin is controlled by the suprachiasmatic nucleus (SCN) in the hypothalamus<sup>4</sup>.

The SCN exerts control over the efferents of the paraventricular nucleus of the hypothalamus, modulating most of the circadian functions of the autonomic nervous system, including the sympathetic pathway whose preganglionic neurons are located in the intermediate lateral column of the spinal cord and which projects to the postganglionic neurons of the superior cervical ganglion. In this pathway, the SCN rhythmically controls the release of noradrenaline, which promotes the activation of the enzyme arylalkylamine N-acetyltransferase (AA-NAT) and consequently the production of melatonin by the pineal gland<sup>5</sup>. In the case of melatonin, its secretion is suppressed by light and stimulated in a dark environment<sup>6</sup>. We also know that melatonin has been reported to be secreted by other organs such as the retina<sup>7-9</sup>, gastrointestinal tract<sup>10</sup>, skin<sup>11</sup>, lymphocytes<sup>12</sup>, and bone marrow<sup>13</sup>. However, the function of melatonin produced outside the pineal does not have a great functional role. It is only a result of the enzymatic degradation of serotonin.

Two subtypes of melatonin receptors have been described: MT<sub>1</sub><sup>14</sup> and MT<sub>2</sub><sup>15</sup>, both of which are G protein-coupled receptors (GPCRs). A third receptor, MT<sub>3</sub>, was later characterized as a reductase enzyme involved in oxidative stress protection events. The localization of MT<sub>1</sub> and MT<sub>2</sub> is not homogeneous. MT<sub>1</sub> is found in many

<sup>1</sup>Departamento de Biofísica e Farmacologia, Universidade Federal do Rio Grande no Norte, Natal, RN 59072-970, Brazil. <sup>2</sup>Bioinformatics Multidisciplinary Environment, Programa de Pós Graduação em Bioinformática, Universidade Federal do Rio Grande do Norte, Natal, RN 59078-400, Brazil. <sup>3</sup>Departamento de Fisiologia e Comportamento, Universidade Federal do Rio Grande no Norte, Natal, RN 59072-970, Brazil. <sup>4</sup>Applied Physics Department, University of Campinas, Campinas, São Paulo 13083-859, Brazil. <sup>5</sup>Unidade Especial de Ciências Exatas, Universidade Federal de Jataí, Jataí, GO 75801-615, Brazil. <sup>6</sup>Laboratório de Pesquisas em Virologia, Departamento de Doenças Dermatológicas, Infecciosas e Parasitárias, Faculdade de Medicina de São José Do Rio Preto, São José Do Rio, Preto, SP 15090-000, Brazil. <sup>7</sup>Centro Nacional de Pesquisa em Energia e Materiais (CNPEM), Brazilian Biosciences National Laboratory, Campinas, SP 13083-100, Brazil. ✉email: umbertofulco@gmail.com

organs and tissues, such as the SCN<sup>16,17</sup>, cerebellum<sup>18</sup>, ovary<sup>19</sup>, testis<sup>19</sup>, liver, kidney, and others<sup>20</sup>. On the other hand, MT<sub>2</sub> is more restricted to the brain, although it has been observed in other tissues such as the lung, heart, and aorta<sup>16</sup>. MT<sub>1</sub> and MT<sub>2</sub> have 350 and 362 amino acids, respectively. They also have 55% sequence homology, and this value increases to 70% when only the transmembrane (TM) region is considered. In terms of function, MT<sub>1</sub>—which has a higher affinity for melatonin—has been shown to acutely suppress neuronal firing, whereas MT<sub>2</sub> is important for efficient phase-shifting<sup>21</sup>.

Structurally, they are also very similar ( $C\alpha$  RMSD < 0.6 Å) and the residues interacting with the binder are conserved<sup>22,23</sup>. Both receptors have the described GPCR configuration: seven transmembrane helices (TM1 to TM7) with an extracellular N-terminus, three extracellular loops (ECL), three intracellular loops (ICL), and a short amphipathic helix VIII, oriented parallel to the membrane<sup>25</sup>. It has been suggested that access to the orthosteric binding site (recognized by melatonin) is via the IV and V helices, which open toward the lipid bilayer<sup>25</sup>.

Currently, there is a high prevalence of sleep disorders in the general population, often associated with work shifts, travel, and mental illnesses such as depression and anxiety<sup>24</sup>. One of these sleep disorders is insomnia, defined as difficulty in initiating or maintaining sleep or constant episodes of non-restorative sleep. It has been described that insomnia affects approximately 30–35% of the adult population and has been associated with an increased risk of mortality. This condition affects both physically and economically those who have it, whether by frequent expenses with doctors and medications or reduction in the working and studying hours due to fatigue<sup>27</sup>. Moreover, studies have linked insomnia with the reduction of cognitive capacity, affecting the retention and manipulation of working memory, problem-solving, and episodic memory<sup>25</sup>. Beyond the cognitive issues, evidence suggests that insomnia increases the risks of developing high blood pressure and type 2 diabetes mellitus<sup>26–28</sup>. Therapeutic interventions for insomnia include both pharmacologic and nonpharmacologic ones, with the latter including lifestyle and behavioral changes such as physical activity, sleep hygiene, sleep restriction, and relaxation therapies<sup>29,30</sup>.

Pharmacological treatment can be divided into two groups of compounds: Benzodiazepines (BZD) and non-benzodiazepines (non-BZD), both of which are sedative-hypnotics.

The BZDs (Estazolam, Flurazepam, Quazepam, or Triazolam) are agents that increase total sleep time and quality of sleep. However, because of adverse effects, such as next-day hangover, amnesia, and potential overuse, these drugs are controversial for long-term treatment of insomnia<sup>31,32</sup>. The non-BZDs (including Zolpidem, Zaleplon, and Eszopiclone) are not as effective as BZDs in improving sleep quality or efficiency, but they are more effective in inducing sleep<sup>33</sup>. In addition, Zolpidem use is associated with other adverse effects such as daytime sleepiness, hallucination, dizziness, headache, nausea, vomiting, and the potential for abuse and dependence<sup>34</sup>.

Despite the adverse effects of BZD and non-BZD, there is increasing interest in the therapeutic use of melatonin to treat insomnia, especially as a sleep inducer. However, the use of melatonin as a medicine has yet to be regulated in several countries, but it is widely used as a food supplement. For example, exogenous melatonin is one of the most popular natural products taken by adults in the United States<sup>35</sup>. The American Academy of Sleep Medicine recommends melatonin for the treatment of circadian rhythm sleep disorder: advanced sleep phase type, free-running (none trained) type in blind adults, and irregular sleep–wake type in children and adolescents with neurological disorders<sup>36</sup>. However, because of its rapid absorption and very short half-life elimination ( $t_{1/2}$ ) from only 40–60 min<sup>37</sup>, it has been suggested that melatonin works best as a chronobiotic rather than a hypnotic<sup>38</sup>, that is, melatonin is effective in regulating the sleep–wake cycle.

To enhance the effectiveness of supplemental melatonin, the production of prolonged-release melatonin—which has a longer duration of action than regular melatonin—emerged as an option. Research has shown that prolonged-release melatonin can increase the sleep duration of people with insomnia<sup>39</sup>. Another way is to use melatonin agonists and analogs, which are compounds that mimic or modify the effects of melatonin on its receptors. Melatonin agonists and analogs have different structures. However, most share a common pharmacophore: an amide group attached to an aromatic ring with a methoxy or a similar group, such as bromine. Some analogs have additional substitutions at the C2 position of the indole ring, which can enhance their affinity for the melatonin receptors by up to 10 times compared to melatonin itself. Examples of these analogs include 2-iodomelatonin and 2-bromomelatonin, which have halogen atoms, 2-phenylmelatonin (2-PMT), which has an aromatic group, and ramelteon (RMT)<sup>40–42</sup>.

Ramelteon<sup>43</sup> was the first melatonin receptor agonist approved by the U.S. Food and Drug Administration (FDA) to treat insomnia associated with difficulty in falling asleep. Compared to melatonin, RMT has six times more affinity for MT<sub>1</sub> receptors and about four times more affinity for MT<sub>2</sub> ones<sup>44</sup>, suggesting that this drug is more suitable for the treatment of insomnia associated with problems in falling asleep<sup>43</sup>. Indeed, studies have shown that taking RMT shortens sleep latency and increases total sleep time and efficiency compared to placebo<sup>45</sup>.

The metabolization of RMT produces four metabolites: M-I, M-II, M-III, and M-IV. In serum, M-II is more abundant than RMT<sup>46,47</sup>. Although M-II exhibits a lower affinity for MT<sub>1</sub> and MT<sub>2</sub> receptors compared to RMT, it also has a longer half-life than melatonin<sup>47</sup>. Overall, the extended half-life of both RMT and its major metabolite, M-II, contributes to their enhanced efficacy compared to melatonin<sup>44</sup>.

RMT also overcomes the adverse effects observed with BZD and non-BZD medications. In the phase I studies, only 5% of the patients discontinued RMT compared to 2% in the placebo group. In phase III, the associated adverse effects were somnolence (0.8%), dizziness (0.5%), nausea (0.3%), fatigue (0.3%), headache (0.3%), and insomnia (0.3%), as described in the manufacturer's prescribing information<sup>48</sup>. In addition, no abuse or dependence potential and no effects on behavior or cognitive performance were observed for RMT<sup>49–52</sup>. Although RMT is an excellent melatonin agonist, it has been used *in silico* studies to obtain new drugs through binder-based drug design. It has also been considered for treating diseases in which melatonin receptor ligands are currently under investigation, including cancer, obesity, diabetes, and pain<sup>53</sup>.

In this context, *in silico* studies have been described as an important initial step in the development of new, more potent drugs based on existing ones<sup>54,55</sup>. These studies involve the analysis of protein–ligand interactions using energetic calculations methodologies through classical mechanics (MM), quantum mechanics (QM), or hybrid methods (QM/MM)<sup>56–59</sup>. This allows for the evaluation of the strengths and weaknesses of each ligand, proposing structural modifications that enhance its affinity for the receptor.

Molecular dynamics (MD) simulations using calculations based on classical mechanics are widely used to obtain optimized structural models of receptor–ligand complexes that are not available in the Protein Data Bank (PDB), especially those obtained through *in silico* molecular docking<sup>60,61</sup>. From the ensemble of conformations generated in MD, protein–ligand interaction calculations can be obtained with relatively low computational cost using methodologies such as Quantum-Mechanical/Molecular-Mechanical Generalized Born Surface Area (QM/MM-GBSA), which is based on the use of semi-empirical functional for quantum mechanics calculations, and classical field force for molecular mechanics calculations.

In this case, semi-empirical methods are reduced-order Hamiltonians in which some elements are replaced by empirical parameters adjusted to experimental or *ab initio* data. Examples include the PM3, PM6, and AM1 models, among others<sup>62,63</sup>. Always aiming for increased accuracy and reduced computational cost, semi-empirical functionals are applied to only a part of the complex (usually defined by the ligand distance), while the remaining is calculated using classical force fields. Despite being a methodology used in drug development studies<sup>64</sup>, it is known that its accuracy is still lower, especially when compared to purely *ab initio* methods such as Density Functional Theory (DFT)<sup>65</sup>.

The DFT emerged as a quantum functional to address the limitations of semi-empirical approaches and other quantum methodologies, such as Hartree–Fock (HF), enabling the study of biological molecules<sup>66,67</sup>. Despite the advantages of DFT, it remains computationally demanding, requiring the use of high-performance clusters and other cost-reduction techniques. One such approach is molecular fragmentation with conjugated caps (MFCC), which involves splitting the system into smaller molecules<sup>71</sup>.

In this aspect, the present work investigates the interaction of two melatonin receptors (MT<sub>1</sub> and MT<sub>2</sub>) complexes with RMT, 2-PMT, and MLT. For this purpose, the crystallographic data of the structural complexes and complexes obtained from docking simulations were used as input geometrical data in the calculation. The quantum binding energy calculations were performed using the DFT formalism DFT in association with the MFCC method. This approach allows us to determine the main contributions of amino acids to their affinity with melatonin receptors.

## Results

### Molecular docking and molecular dynamics simulation

To obtain the MT<sub>1</sub>-MLT and MT<sub>2</sub>-MLT complexes, molecular docking was performed using AutoDock Vina<sup>68</sup>. The distribution of Vina scores (in kcal/mol) from 1000 rounds of docking can be observed in Fig. 1A, and a

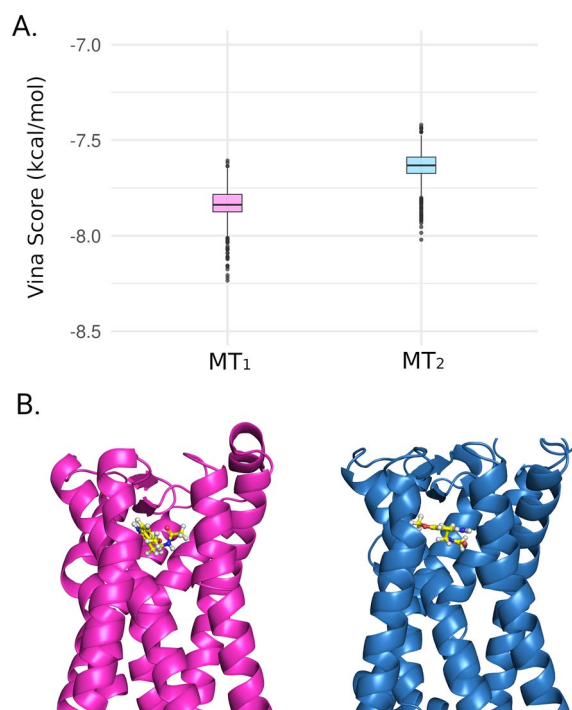


**Figure 1.** Melatonin docking in MT<sub>1</sub> and MT<sub>2</sub>. (A) Box plot of Vina score distribution in kcal/mol. The pink box is related to MT<sub>1</sub>-MLT complex and the blue is related to MT<sub>2</sub>-MLT docking. (B) Best docking pose of MLT (yellow stick) bound in MT<sub>1</sub> (pink cartoon) and MT<sub>2</sub> (blue cartoon).

summary of the obtained values is presented in Table 1. The Vina scores for the MT<sub>1</sub>-MLT complex ranged from  $-7.607$  kcal/mol to  $-8.235$  kcal/mol, with a mean (SD) value of  $-7.832$  kcal/mol (0.08753). Similarly, for the MT<sub>2</sub>-MLT complex, the Vina scores ranged from  $-7.420$  kcal/mol to  $-8.021$  kcal/mol, with a mean (SD) of  $-7.632$  kcal/mol (0.07979). These results indicate that melatonin has a higher affinity for the MT<sub>1</sub> protein compared to MT<sub>2</sub>. However, it is important to note that the primary objective of the exhaustive Vina docking is to rank the complexes based on Vina scores. Furthermore, as depicted in Fig. 1B, the best MLT conformations bind to the same pocket as observed in experimental structures<sup>23</sup>, further confirming the reliability of the docking results. Therefore, the obtained data strongly suggest that the docking results are suitable for proceeding to MD simulations.

The main purpose of the MD simulations is to adjust the conformation of the protein and ligand in a solvent environment. The Root Mean Square Deviation (RMSD) is a metric that evaluates the difference between 3D structures based on atomic distances. A higher RMSD value indicates a greater difference in structures. In this study, we compared the structures along the trajectory with the initial frame. The RMSD of the MT<sub>1</sub>-MLT complex can be seen in Fig. 2A. It is noteworthy that all three replicates exhibited similar behavior throughout the 200 ns trajectory, with an RMSD value of approximately 0.5 nm. Additionally, the Root Mean Square Fluctuation (RMSF) analysis (Fig. 2C), which evaluates the average residue fluctuation, showed no significant differences among the three replicates. It is expected to observe higher fluctuation in the N- and C-termini of the protein. However, in this case, only higher residue fluctuation was observed in the C-terminal region of the protein.

Unlike the MT<sub>1</sub>-MLT complex, the three replicates of MT<sub>2</sub>-MLT exhibited distinct behaviors along the MD trajectory. Among them, the RMSD (Fig. 2B) of replicate 2 was more stable. Like MT<sub>1</sub>-MLT, the RMSD value remained around 0.5 nm. In contrast, replicate 3 showed a higher but stable RMSD (0.65 nm) until 125 ns into the simulation. Afterward, the RMSD increased to values higher than 1.1 nm, and after 150 ns, stability was observed near this RMSD value. The heatmap plot of RMSD per residue over time (Supplementary Figure S1C) revealed an increasing fluctuation of residues attached in the MT<sub>2</sub> N-terminal, which corresponds to the apocytochrome BRIL (UniProt P0ABE7) from *Escherichia coli*, after 125 ns. Additionally, around 60 ns, an increased RMSD in residues of MT<sub>2</sub> C-terminal corresponding to another fusion protein, rubredoxin (Rub, UniProt P00268). Notably, these residues are distant from the ligand binding pocket, suggesting that they have insignificant influence on the ligand binding mode. Finally, replicate 1 showed intermediate fluctuations with values near 0.8 nm until 175 ns, followed by a small decrease to values near 0.70 nm. The fusion protein also observed these variations, as shown in Supplementary Figure S1A. The structure of MT<sub>2</sub> and the fusion proteins can be seen in Supplementary Figure S2. The RMSF analysis of the MT<sub>2</sub> replicas (Fig. 2D) indicates that the fluctuation patterns were quite similar among them, despite the amplitude of replica 3 being larger, which corroborates with the observations made in the RMSD graph. Conversely, the fluctuations of replicas 1 and 2 were alike in terms of both amplitude and fluctuation pattern.

Protein	Vina Score (kcal/mol)						
	Min	1st quartile	Median	Mean	3rd. quartile	Máx	sd <sup>†</sup>
MT <sub>1</sub>	-8.235	-7.875	-7.838	-7.832	-7.784	-7.607	0.08753
MT <sub>2</sub>	-8.021	-7.674	-7.632	-7.640	-7.589	-7.420	0.07979

**Table 1.** Summary of Vina docking results based on 1000 ligand conformations. <sup>†</sup>sd: standard deviation.

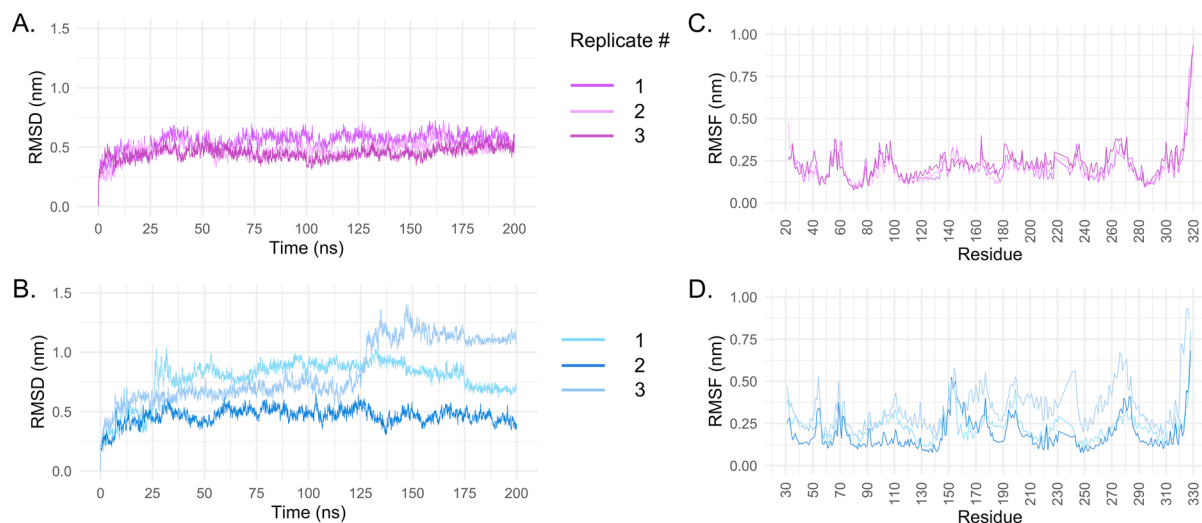


**Figure 2.** RMSD and RMSF analysis of 200 ns three MD trajectory. (A) and (B) RMSD plots in three replicates of MT<sub>1</sub> and MT<sub>2</sub> MD simulations, respectively. (C) and (D) RMSF plots in three replicates of MT<sub>1</sub> and MT<sub>2</sub> by residue number, respectively.

The RMSD analysis of the ligand is an interesting means to evaluate if the ligand remained in the binding pocket or if displacement occurred. A high RMSD indicates a modification in the ligand's position. Supplementary Figure S3 shows that MLT in complex with MT<sub>1</sub> and MT<sub>2</sub> remained in the pocket as the RMSD did not show high values. However, MLT in MT<sub>1</sub> showed an RMSD near 0.5 nm, while MLT in MT<sub>2</sub> showed an RMSD near 0.8 nm, suggesting that MLT-MT<sub>2</sub> underwent a higher conformational change during the MD simulation compared to MLT-MT<sub>1</sub>. These results were found to be suitable for performing the QM/MM-GBSA analysis.

The results of QM/MM-GBSA can be observed in Table 2 and Fig. 3. In Table 2, it is possible to observe that the mean of all replicas showed lower energy in the interaction with MLT for MT<sub>1</sub> compared to MT<sub>2</sub>, except for replica 3. This is also true when we compare the lowest value for each replicate. Notably, the QM/MM-GBSA analysis of MT<sub>1</sub>-MLT (Fig. 3A) showed more variation among replicates compared to the MT<sub>2</sub>-MLT complex. However, both complexes exhibited values mostly lower than -10 kcal/mol. As observed in the Vina docking results, the complex with higher affinity was MT<sub>1</sub>-MLT. The selected frames for MFCC/DFT analysis were frame 1648 (replicate 2, MT<sub>1</sub>), which presented -27.57 kcal/mol of binding energy, and frame 1871 (replicate 2, MT<sub>2</sub>) which presented -24.78 kcal/mol of energy. Now, there are six complexes for which QM calculations will be performed: MT<sub>1</sub>-MLT, MT<sub>2</sub>-MLT, MT<sub>1</sub>-RMT, MT<sub>2</sub>-RMT, MT<sub>1</sub>-2-PMT, and MT<sub>2</sub>-2-PMT. The last four complexes were obtained from the Protein Data Bank (accession codes: 6ME2, 6ME9, 6ME3 and 6ME6 respectively).

The structures of MT<sub>1</sub>-MLT and MT<sub>2</sub>-MLT selected for QM (DFT) calculations were compared with their experimentally resolved counterparts, both in their active and inactive forms. The structure of MT<sub>1</sub>-MLT was compared with structures PDB ID: 7DB6<sup>73</sup> (active, Cryo-EM) and PDB ID: 6ME2<sup>25</sup> (inactive, X-ray) and the complex MT<sub>2</sub>-MLT was overlaid with structures PDB ID: 7VH0<sup>69</sup> (active, Cryo-EM) and 6ME6<sup>23</sup> (inactive, X-ray). As observed in Fig. 4A, a displacement of TM6 in the active state (light blue ribbon) is noted when compared to MT<sub>1</sub> with MLT (light green ribbon). The same is observed in MT<sub>2</sub>-MLT (Fig. 4B). Figure 4C and D present the overlay of MT<sub>1</sub>-MLT and MT<sub>2</sub>-MLT with inactive MT<sub>1</sub> and MT<sub>2</sub>, respectively. It is noted that the displacement of TM6 when comparing the complexes with each other is much smaller, indicating that the complex with MLT is anchored in the inactive form of the melatonin receptor. This is expected since the docking was performed with the protein in this conformation. Therefore, it is concluded that the MD simulation maintained the complex in its inactive state.

### MFCC and quantum mechanical calculations

To aid in examining and analyzing binder interactions, we schematically divided the binders into regions, as illustrated in Fig. 5. The carbon atoms are labeled from 1 to 19, and the rings are denoted by letters (A, B, and C). According to the Marvin Sketch analysis, neutral states were predominant (100%) at both pH values examined (7.0 and 7.4). In Fig. 5B, the MT<sub>1</sub> and MT<sub>2</sub> receptors are represented with the RMT and 2-PMT molecules, respectively, highlighting the binding site of the ligands.

Energy calculations and evaluations were performed for each of the six complexes, and convergence criteria were determined based on the variation of total energy (in kcal/mol) and radius *r* (in Å). The cumulative binding

Protein	Replicate 1		Replicate 2		Replicate 3	
	Mean ± sd <sup>†</sup>	Lowest value	Mean ± sd <sup>†</sup>	Lowest value	Mean ± sd <sup>†</sup>	Lowest value
MT <sub>1</sub>	-17.07 ± 3.01	-26.07	-18.88 ± 2.94	-27.57	-13.00 ± 2.72	-22.26
MT <sub>2</sub>	-10.81 ± 2.23	-16.92	-16.08 ± 2.87	-24.78	-14.82 ± 2.60	-22.84

**Table 2.** QM/MM results of MT<sub>1</sub>-MLT and MT<sub>2</sub>-MLT complexes.

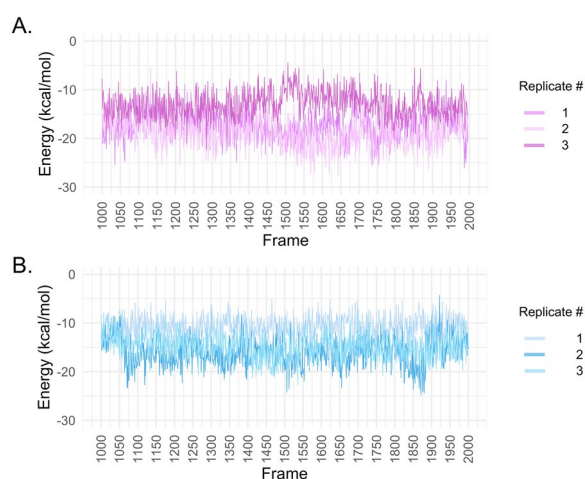


**Figure 3.** QM/MM values along trajectory frames (A). MT<sub>1</sub> three replicates. (B) MT<sub>2</sub> replicates.



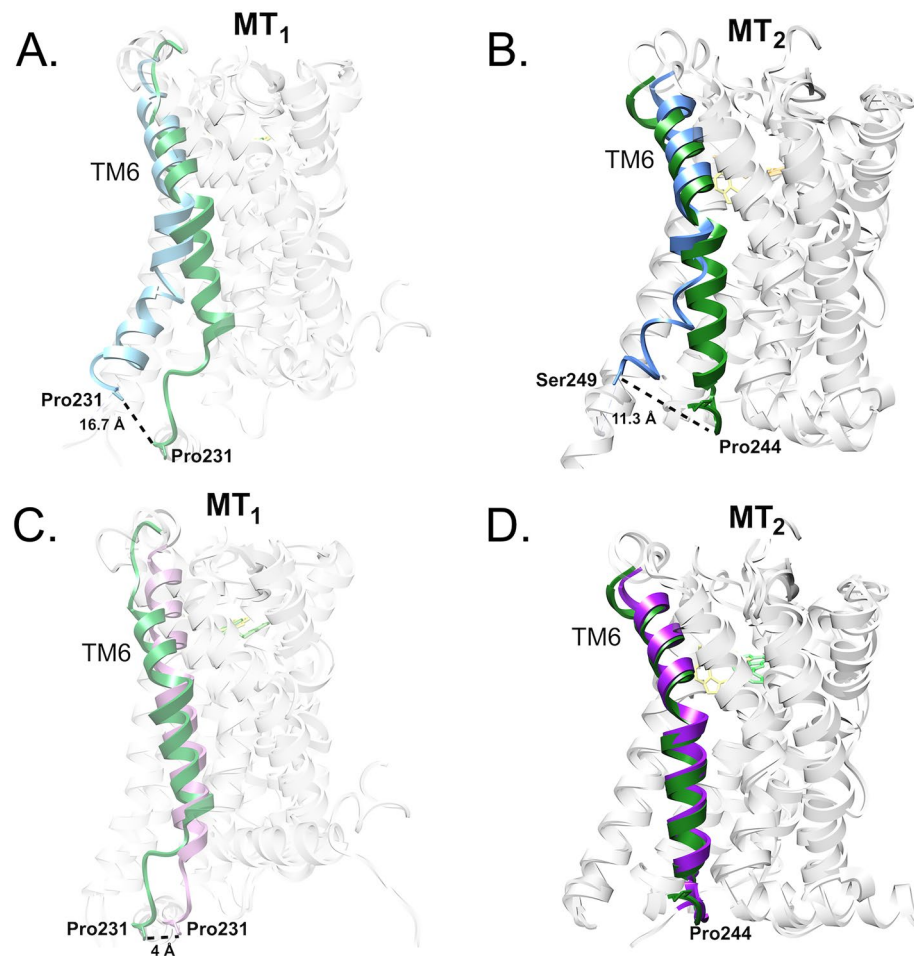


**Figure 4.** Comparison of the MT<sub>1</sub> and MT<sub>2</sub> structures in their active and inactive forms. **(A)** Comparison of the active MT<sub>1</sub> structures (blue color ribbon) with the MT<sub>1</sub>-MLT complex (green color ribbon). **(B)** Comparison of the active MT<sub>2</sub> (blue color ribbon) with the MT<sub>2</sub>-MLT complex (green color ribbon). **(C)** Comparison of the inactive MT<sub>1</sub> structures (pink color ribbon) with the MT<sub>1</sub>-MLT complex (green color ribbon). **(D)** Comparison of the inactive MT<sub>2</sub> structures (purple color ribbon) with the MT<sub>2</sub>-MLT complex (green color ribbon).

energy was obtained by summing up all the calculated energies between the residues within the radius and the binder. The analyses were continued until the contributions of amino acids from each radius were no longer significantly different from the total interaction energy found after each successive radius, with a threshold of less than 10%.

Figure 6 illustrates the change in total interaction energy with increasing radius. The convergence criteria are met between  $r = 7 \text{ \AA}$  and  $8 \text{ \AA}$  for all complexes and dielectric constants ( $\epsilon = 10$  and  $\epsilon = 40$ ). However, calculations were conducted within  $r = 10 \text{ \AA}$  to ensure the comprehensive evaluation of crucial residues. As a result, for the MT<sub>1</sub>-RMT and MT<sub>2</sub>-RMT complexes, 96 and 105 residues were found to interact within  $r = 10 \text{ \AA}$ , respectively. In terms of affinity, the total interaction energy when  $\epsilon = 40$  ( $\epsilon = 10$ ) for MT<sub>1</sub>-RMT was  $-43.08 \text{ kcal/mol}$  ( $-43.84 \text{ kcal/mol}$ ) and for MT<sub>2</sub>-RMT  $-48.75 \text{ kcal/mol}$  ( $-50.07 \text{ kcal/mol}$ ), suggesting that the RMT drug has a slightly higher affinity for MT<sub>2</sub>-RMT. In the case of MT<sub>1</sub>-2-PMT and MT<sub>2</sub>-2-PMT, binding affinity was assessed for 104 and 108 residues, respectively. The total energies for these residues were  $-60.09 \text{ kcal/mol}$  ( $-61.54 \text{ kcal/mol}$ ) for MT<sub>1</sub>-2-PMT and  $-54.71 \text{ kcal/mol}$  ( $-56.49 \text{ kcal/mol}$ ) for MT<sub>2</sub>-2-PMT, when  $\epsilon = 40$  ( $\epsilon = 10$ ). For the MT<sub>1</sub>-MLT and MT<sub>2</sub>-MLT complexes revealed interactions with 86 residues within  $r = 10 \text{ \AA}$ . In terms of affinity, the total interaction energy for MT<sub>1</sub>-MLT was  $-50.01 \text{ kcal/mol}$  ( $-51.53 \text{ kcal/mol}$ ) and for MT<sub>2</sub>-MLT was  $-44.26 \text{ kcal/mol}$  ( $-45.13 \text{ kcal/mol}$ ), with dielectric constants  $\epsilon = 40$  ( $\epsilon = 10$ ).

Based on the data above, it is observed that the increasing order of affinity of the MT<sub>1</sub> (MT<sub>2</sub>) receptor is: RMT < MLT < 2-PMT (MLT < RMT < 2-PMT), which suggests that 2-PMT acts better on both receptors compared to RMT and MLT. Moreover, all energy values show what is expected for  $\epsilon = 10$  compared to  $\epsilon = 40$ , where the first shows lower values due to increased medium permittivity. Furthermore, it is observed that the pattern for  $\epsilon = 10$  and  $\epsilon = 40$  remained consistent in the plots, which strongly suggests that the DFT calculations were carried out correctly. Therefore, from now on, we will present the study with energy results focused on the dielectric constant  $\epsilon = 40$ .

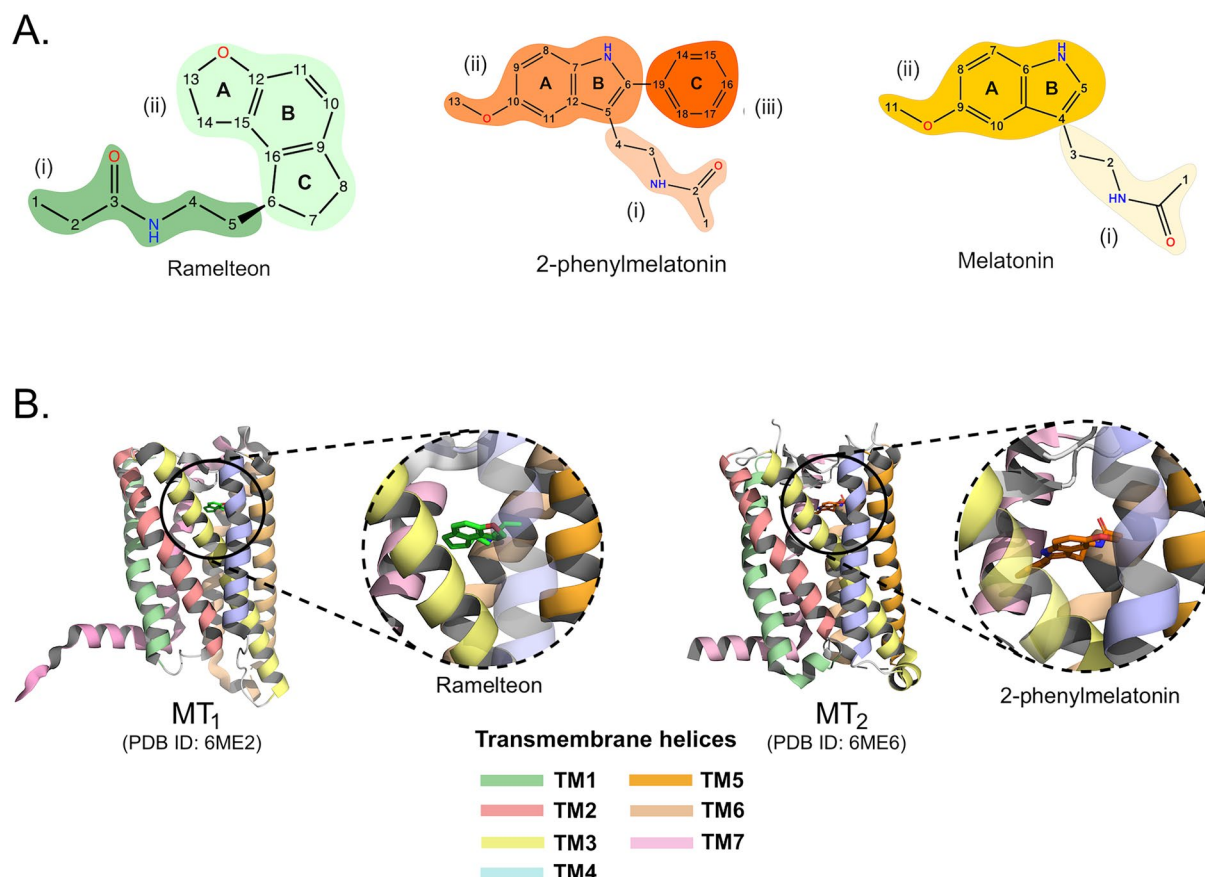


**Figure 5.** (A) Schematic representation of 2D structure of Ramelteon (green), 2-phenylmelatonin (orange) and Melatonin (yellow). (B) Structures of the MT<sub>1</sub> complexed with RMT (green stick) and MT<sub>2</sub> complexed with 2-PMT (orange stick) to 7/20 illustrate the binding site of the three binders.

#### MT<sub>1</sub> interaction analysis

The individual energetic contribution of each amino acid was evaluated to understand the most significant residues in the interaction with MT<sub>1</sub>, as well as the ligand regions where these interactions occurred. In Fig. 7, the calculated energy of the key amino acids that contributed (both positively and negatively) to the interaction energy between the complexes can be observed. For interactions within the MT<sub>1</sub>-RMT complex (Fig. 7, green bar), the ten most important residues in decreasing order of affinity (in kcal/mol) are the following: Phe179 (−7.93) > Met107 (−3.83) > Val191 (−3.15) > Gly108 (−2.51) > Val111 (−2.25) > Gln181 (−2.13) > Tyr281 (−2.04) > Ile112 (−1.93) > Val159 (−1.86) > Asn162 (−1.32). Despite its very small energy value, Leu254 was the only residue shown in Fig. 7 to exhibit a negligible repulsive affinity (0.05 kcal/mol). For MT<sub>1</sub>-2-PMT (Fig. 7, orange bar), following the same order, these residues were: Phe179 (−9.21) > Gln181 (−4.57) > Leu254 (−4.32) > Met107 (−3.70) > Gly108 (−3.53) > Val111 (−3.39) > Val191 (−3.13) > Tyr281 (−3.05) > Thr178 (−2.55) > Tyr285 (−2.28) > Val159 (−2.10) > Ile112 (−2.01) > Phe251 (−1.77) > Asn255 (−1.71). In the case of MT<sub>1</sub>-MLT (Fig. 7, yellow bar), the main residues in descending order of affinity (in kcal/mol, for  $\epsilon = 40$ ) were: Phe179 (−7.04) > Val159 (−4.30) > Asn162 (−4.15) > Ile112 (−3.31) > Gly108 (−3.05) > Ala104 (−2.72) > Leu168 (−2.38) > Thr178 (−2.33) > Phe105 (−2.14) > Leu254 (−2.0) > Met107 (−1.93) > Val111 (−1.89) > Val191 (−1.67). Seven common amino acid residues were observed between them: Phe179, Met107, Gly108, Val111, Val191, Val159, and Ile112. These residues are then suggested as key interacting residues, and main interactions with them will be evaluated in detail.

Phe179 was the most important residue for interaction in all three MT<sub>1</sub> complexes. It formed a pi-alkyl interaction with atom [ii(C8)] of the RMT molecule (Fig. 8A) and two pi-pi interactions with rings [A,B] of 2-PMT (Fig. 8B) and MLT (Fig. 8C). Interestingly, Phe179 showed high affinity for ligands (between −7.04 kcal/mol to −9.21 kcal/mol) regardless of whether they interacted with its aromatic ring or aliphatic carbon. Val159 interacted with atoms from the aromatic region of RMT and 2-PMT (Fig. 8A-B) through dipole-dipole interactions. In contrast, it formed a non-conventional hydrogen bond with MLT (Fig. 8C), which resulted in a higher affinity interaction (−4.30 kcal/mol) than the other molecules. Ile112 exhibited dipole-dipole interactions with all molecules. However, the interaction energies were lower for RMT (Fig. 8A) and 2-PMT (Fig. 8B) (−1.93 kcal/mol and −2.01 kcal/mol, respectively) than for MLT (Fig. 8C) (−3.31 kcal/mol). This could be attributed to the distance factor, as Ile112 interacted with the same shared region of MLT (2.8 Å) and 2-PMT (3.6 Å). For RMT, the interaction involved a hydrogen atom bonded to a carbon atom of the aromatic ring [ii(C14)H], which may have affected the charge distribution and attractive forces.

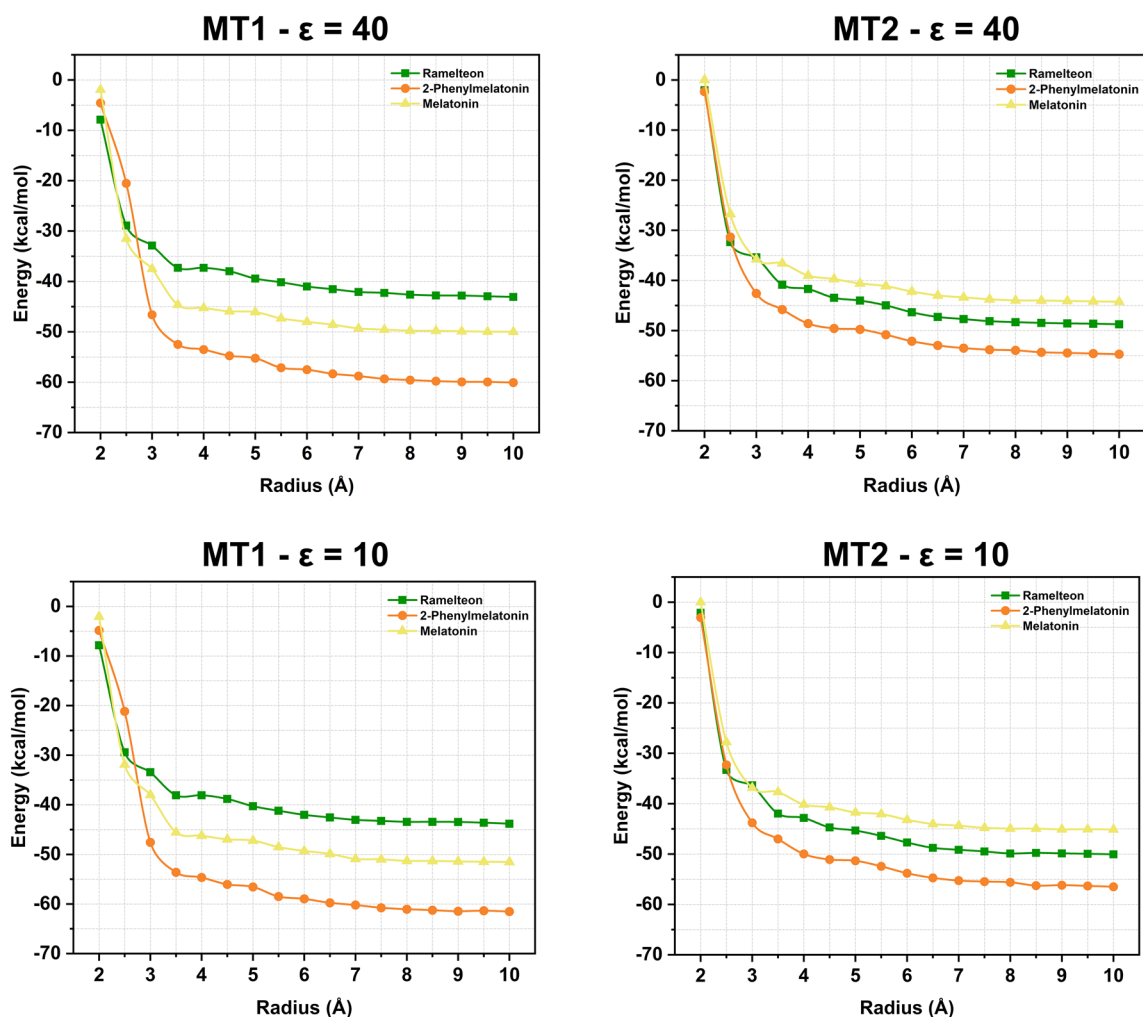


**Figure 6.** Plot representation of total interaction energy of  $MT_1$  and  $MT_2$  complexes for both dielectric constants ( $\epsilon = 10$  and  $\epsilon = 40$ ) as a function of the binding pocket radius calculated using the DFT/MFCC approach.

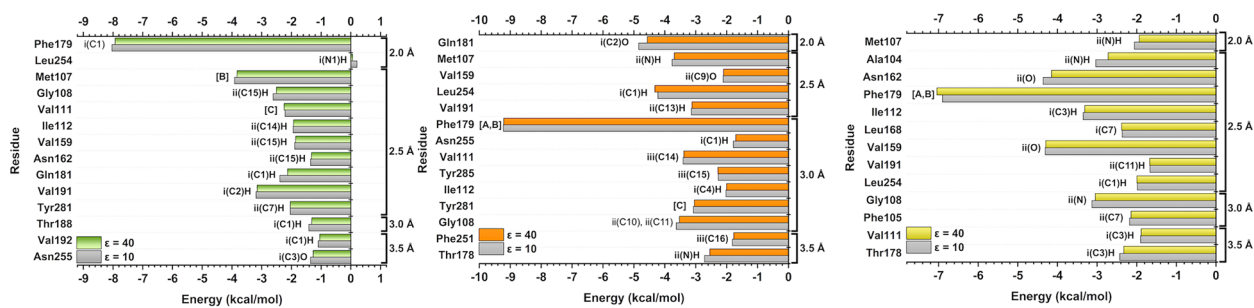


**Figure 7.** Graphic panels showing the most important residues for  $MT_1$  interaction with RMT (green bar), 2-PMT (orange bar) and MLT (yellow bar). Also, the region (i, ii or iii) and atom (based on Fig. 5 schematic representation) that interact with each residue at the binding site.

Met107 was another important key residue for interaction with all ligands. It showed lower energy values for RMT ( $-3.83$  kcal/mol) (Fig. 8D) and 2-PMT ( $-3.70$  kcal/mol) (Fig. 8E) than for MLT ( $-1.93$  kcal/mol) (Fig. 8F). It formed a pi-sulfur interaction with ring [B] of RMT (Fig. 8D), a dipole-dipole interaction and a non-conventional hydrogen bond with atom [ii(N)H] of 2-PMT (Fig. 8E), and a dipole-dipole interaction with atom [ii(N)H] of MLT (Fig. 8F). RMT did not meet the non-conventional hydrogen bond parameters. Val111 performed pi-alkyl interactions with aromatic rings of RMT (Fig. 8D) and 2-PMT (Fig. 8E), which resulted in higher affinity than its dipole-dipole interaction with MLT (Fig. 8F). Gly108 exhibited considerable affinity for all ligands. It formed dipole-dipole interactions with atoms [ii(C15)H] of RMT (Fig. 8D), [ii(C10) and ii(C11)] of 2-PMT (Fig. 8E), and [ii(N)] of MLT (Fig. 8F). The latter was also a hydrogen bond. Finally, Val191 showed



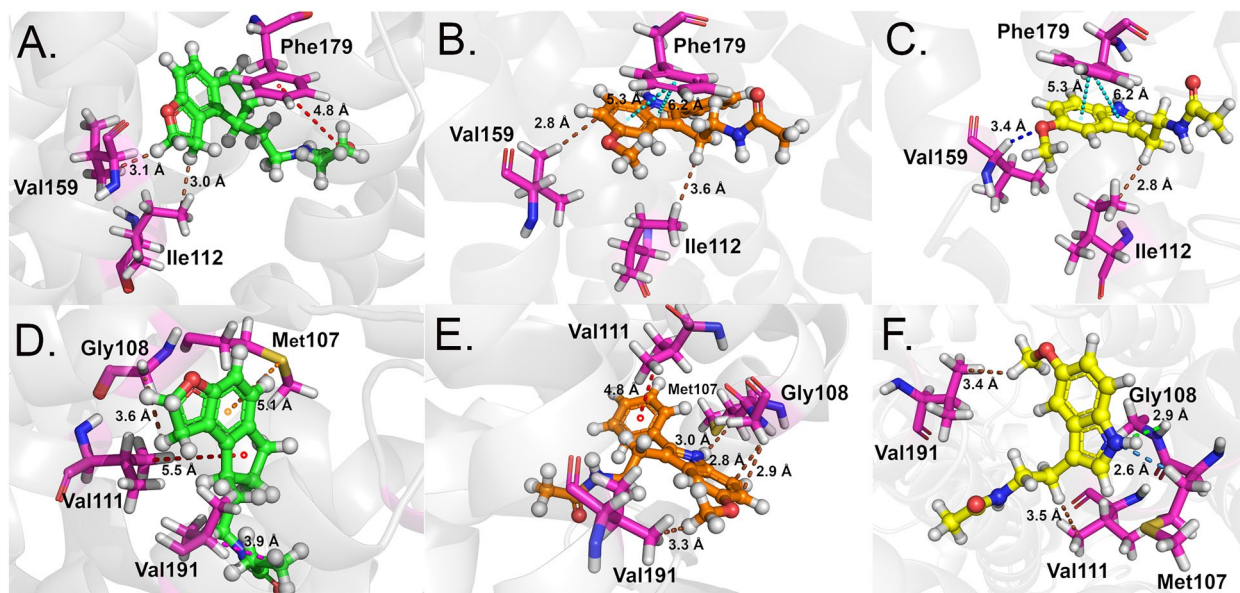


**Figure 8.** Tri-dimensional binding mode of RMT (A and D), 2-PMT (B and E) and MLT (C and F) in MT<sub>1</sub> structure. The ligands are represented in ball and stick (RMT—green, 2-PMT—orange and MLT—yellow) and the main MT<sub>1</sub> amino acids in magenta sticks. The interaction types are colored as follows—green: hydrogen bond; cyan: pi-pi interaction; dark blue: non-conventional hydrogen bond; brown: dipole-dipole; red: pi-alkyl; orange: pi-sulfur.

higher affinity for RMT (−3.15 kcal/mol) and 2-PMT (−3.13 kcal/mol) than for MLT (−1.67 kcal/mol). It formed an alkyl-alkyl interaction with an atom [i(C2)H] of RMT and dipole-dipole interactions with atoms [ii(C13)H] of 2-PMT and [ii(C11)H] of MLT.

#### MT<sub>2</sub> interaction analysis

Among the residues of MT<sub>2</sub>-RMT complex (Fig. 9, green bar), the ten residues that most contributed to the binding affinity in decreasing order (in kcal/mol) were: Phe192 (−9.95) > Gln194 (−3.72) > Gly121 (−3.22) > Val204 (−3.05) > Met120 (−2.99) > Asn175 (−2.84) > Val124 (−2.56) > Leu172 (−2.25) > Asn268 (−1.91) > Leu267 (−1.86). Similar to MT<sub>1</sub>-RMT complex, only one residue (Ala117) showed repulsive energy (1.26 kcal/mol) for the binder. In the case of MT<sub>2</sub>-2-PMT (Fig. 9, orange bar), these residues are: Phe192 (−9.22) > Val124 (−4.12) > Tyr294 (−4.07) > Leu267 (−3.59) > Gly121 (−3.19) > Asn175 (−2.76) > Val204 (−2.69) > Thr191 (−2.32) > Ile125 (−2.11) > Met120 (−2.06) > Tyr298 (−2.05) = Phe264 (−2.05) > Leu172 (−1.79) > Asn268 (−1.69) > Ala117 (2.64). It is noteworthy that only the Ala117 residue in the MT<sub>2</sub>-2-PMT complex showed positive energy, indicating a repulsive interaction. When observing key residues in the MT<sub>2</sub>-MLT interaction (Fig. 9, yellow bar), the following amino acids were found to be significant for interaction energy (in kcal/mol, for  $\epsilon = 40$ ): Leu267 (−6.01) > Val204 (−4.48) > His208 (−3.87) > Val205 (−3.79) > Val124 (−2.84) > Phe209 (−2.65) > Ile125 (−2.24) > Leu172 (−2.24) > Asn268 (−1.80) > Phe192 (−1.79) > Gly121 (−1.09). In common, six key residues were observed: Phe192, Val124, Gly121, Val204, Leu172, and Asn268.

As observed for MT<sub>1</sub>, Phe192 of MT<sub>2</sub> structure had the highest affinity for RMT (−9.95 kcal/mol) and 2-PMT (−9.22 kcal/mol). It formed two pi-pi interactions with two aromatic rings of each ligand (Fig. 10A–B). In the MT<sub>2</sub>-MLT complex, Phe192 had a lower energy value (−1.79 kcal/mol) and a dipole-dipole interaction with atom [i(C1)H] (Fig. 10C). Val124 performed a pi-alkyl interaction with RMT (−2.56 kcal/mol), a pi-sigma interaction

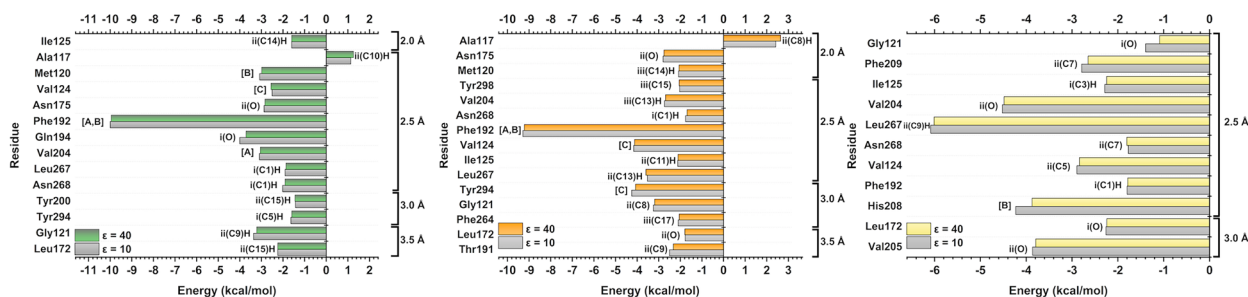


**Figure 9.** Graphic panels showing the most important residues for MT<sub>2</sub> interaction with RMT (green bar), 2-PMT (orange bar) and MLT (yellow bar). Also, the region (i, ii or iii) and atom (based on Fig. 5 schematic representation) that interact with each residue at the binding site.

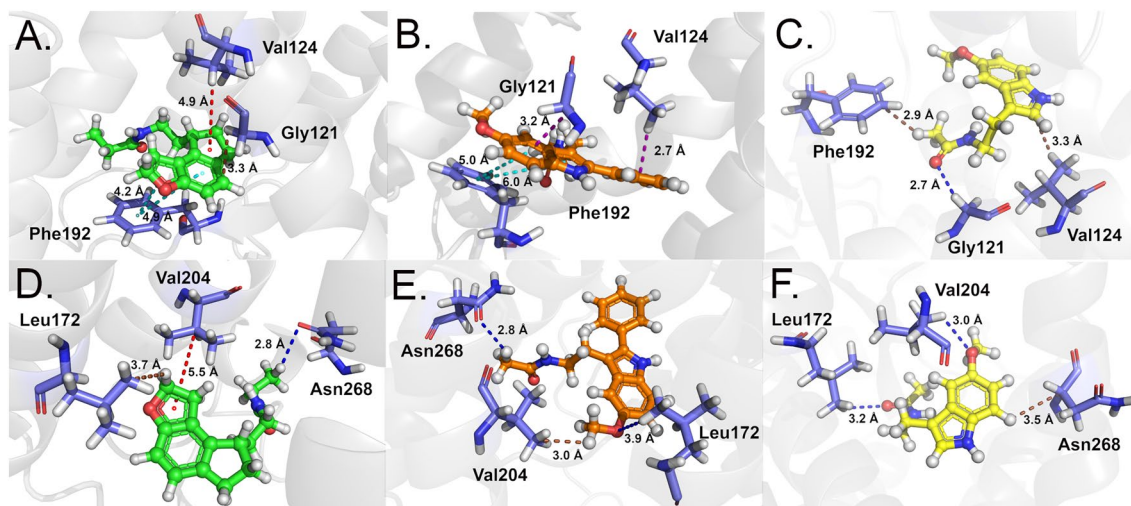


**Figure 10.** Tri-dimensional binding mode of RMT (A and D), 2-PMT (B and E) and MLT (C and F) in  $MT_2$  structure. The ligands are represented in ball and stick (RMT—green, 2-PMT—orange and MLT—yellow and the main  $MT_2$  amino acids in blue sticks. The interaction types are colored as follows—cyan: pi–pi interaction; dark blue: non-conventional hydrogen bond; brown: dipole–dipole; red: pi-alkyl; purple: pi-sigma.

with the aromatic ring of 2-PMT (–4.12 kcal/mol), and a dipole–dipole interaction with atom [ii(C5)] of MLT (–2.84 kcal/mol) (Fig. 10A–C). Gly121 showed affinity energies lower than –3.0 kcal/mol for RMT and 2-PMT (–3.22 kcal/mol and –3.19 kcal/mol, respectively). It formed a dipole–dipole interaction with atom [ii(C9)H] of RMT and a non-conventional hydrogen bond with atom [ii(N)] of 2-PMT (Fig. 10A,B). For MLT (–1.09 kcal/mol), it formed a non-conventional hydrogen bond with atom [i(O)] (Fig. 10C).

Val204 had a higher affinity for MLT (–4.48 kcal/mol) than for RMT (–2.69 kcal/mol) and 2-PMT (–2.69 kcal/mol). It formed a pi-alkyl interaction with ring [C] of RMT (Fig. 10D), a dipole–dipole interaction with atom [iii(C13)H] of 2-PMT (Fig. 10E), and a non-conventional hydrogen bond with atom [ii(O)] of MLT (Fig. 10F). The latter favored its increased affinity. Asn268 formed non-conventional hydrogen bonds with atom [i(C1)H] of both RMT (–1.91 kcal/mol) and 2-PMT (–1.69 kcal/mol) (Fig. 10D,E). With MLT, it formed a dipole–dipole interaction with atom [ii(C7)], and the calculated energy was –1.80 kcal/mol (Fig. 10F). Finally, Leu172 formed a dipole–dipole interaction with atom [ii(C15)H] of RMT (–2.25 kcal/mol) (Fig. 10D) and non-conventional hydrogen bonds with 2-PMT (–1.79 kcal/mol) and MLT (–2.24 kcal/mol) (Fig. 10E,F).

### Alanine scanning

The alanine scanning study is an exciting approach to assessing the significance of amino acids in protein–ligand complexes. The PremPLI server, a straightforward tool based on machine learning, predicts the mutation's effect solely using 3D structural information from the complex. In this case, the evaluated interactions involved the amino acids Gly108/Gly121, Val111/Val124, and Val191/Val204 across all ligands (RMT, 2-PMT, and MLT). The analysis of amino acids Gln181/194, Phe179/192, and Asn162/175 was restricted to those ranked with low energy according to QM/DFT calculations.

As seen in Table 3, the mutation with the most significant impact on interaction reduction was F179A/F192A. The highest quantum calculations energy for Phe192 was associated with the MLT ligand, and according to PremPLI, it also exhibited the most negligible impact on the mutation. Notably, among the amino acids Gly108/Gly121, Val111/Val124, and Val191/Val204, the G108A/G121A mutation had the most substantial impact on interaction, according to PremPLI. However, it is observed that in all complexes, the mutations resulted in positive  $\Delta\Delta G$  values, indicating reduced affinity.

Despite PremPLI's results aligning with QM calculations, further robust analyses are essential to confirm the importance of amino acids Gly108/Gly121, Val111/Val124, and Val191/Val204 in ligand recognition and interaction with  $MT_1$  and  $MT_2$  receptors.

### Discussion

The search for new therapeutic strategies for the treatment of insomnia has become extremely important, mainly due to the various adverse effects caused by the use of BZDs and n-BZDs drugs in the general population. Several agonists and analogs of MLT have been studied for years, such as RMT, 2-iodomelatonin, agomelatonin, and 2-PMT<sup>23</sup>. However, all these drugs were developed before the three-dimensional resolution of the  $MT_1$  and  $MT_2$  receptors, using the ligand-based drug discovery (LBDD) strategy.

Thanks to the recent advances in the resolution of the structures of the  $MT_1$  and  $MT_2$  proteins, it is now possible to meticulously evaluate the interactions between the receptors and their ligands. Therefore, this study was developed to fill two gaps related to the melatonin receptors: to obtain a model with MLT and its receptors and to evaluate the biochemical interactions with RMT, 2-PMT, and MLT to propose a structure-based drug discovery (SBDD) strategy, which is reported to be more complex and potentially better than LBDD<sup>70</sup>. The

Protein	Ligand	Mutation	$\Delta\Delta G$	QM/DFT (kcal/mol)	Protein	Ligand	Mutation	$\Delta\Delta G$	QM/DFT (kcal/mol)
MT <sub>1</sub>	RMT	F179A	1.17	-7.93	MT <sub>2</sub>	RMT	F192A	1.21	-9.95
		Q181A	1.04	-2.39			Q194A	0.99	-3.72
		N162A	0.82	-1.36			N175A	1.25	-2.84
		G108A	0.99	-2.61			G121A	1.03	-3.22
		V111A	0.7	-2.21			V124A	0.64	-2.56
		V191A	0.63	-3.19			V204A	0.6	-3.05
	2-PMT	F179A	1.28	-9.21		2-PMT	F192A	1.36	-9.22
		Q181A	0.73	-4.57			N175A	1.02	-2.76
		G108A	1.07	-3.53			G121A	0.93	-3.19
		V111A	0.43	-3.39			V124A	0.47	-4.12
		V191A	0.54	-3.13			V204A	0.44	-2.69
	MLT	F179A	1.4	-6.9		MLT	F192A	1.03	-1.79
		N162A	0.71	-4.36			G121A	0.85	-1.09
		G108A	0.97	-3.13			V124A	0.57	-2.64
		V111A	0.21	-1.9			V204A	0.66	-4.48
V191A		0.23	-1.66						

**Table 3.** Results of alanine scanning performed by the PremPLI server for the key amino acids indicated by QM/DFT calculations.

docking analysis allowed the orientation of MLT in the MT<sub>1</sub> and MT<sub>2</sub> receptors to be predicted *in silico*, since the structures of the experimental complexes are not yet available. Thus, it was possible to determine how MLT interacts with its receptors. The MD simulation provided important information regarding the stability of MLT in solution when bound to the MT<sub>1</sub> and MT<sub>2</sub> receptors. This is crucial because a molecule that does not stabilize in the active site of the protein with the conformational changes observed in solution does not become a suitable therapeutic target for use.

In this study, we can observe that MLT has good stability when complexed with its targets. In the docking and MD simulation study, it was possible to obtain complexes of MT<sub>1</sub>-MLT and MT<sub>2</sub>-MLT in their inactive state, as well as the other structures analyzed in this study. This comparison was feasible because the TM6 domain in the active form exhibits a displacement relative to the inactive form, which is well described by previous studies with experimentally resolved structures<sup>69</sup>.

In the QM/DFT analysis using the MFCC method, it was observed that the increasing order of affinity for MT<sub>1</sub> was RMT < MLT < 2-PMT, which suggests that 2-PMT is the best ligand for MT<sub>1</sub> activation and RMT is the weaker. In the case of MT<sub>2</sub> this order was: MLT < RMT < 2-PMT, which suggests again 2-PMT as the best binder, however, in this case, MLT was ranked as the weaker MT<sub>2</sub> ligand. All ligands showed higher affinity for MT<sub>1</sub> compared to MT<sub>2</sub>, except the RMT binder. The 2-PMT and MLT results corroborate with *in vitro* experimental data where the affinity of 2-PMT and MLT for the receptors was evaluated. In these studies, it is possible to observe that the affinity of 2-PMT is higher than the affinity of MLT<sup>71</sup> for both receptors, and both molecules have a higher affinity for MT<sub>1</sub> than for MT<sub>2</sub><sup>71-73</sup>. The RMT results do not agree with the experimental data. Further analysis should be performed to evaluate if this is a limitation of the calculation method or the experimental crystallographic data. However, most of the results shown here are in agreement with *in vitro* tests.

In the literature, the importance of three amino acids for protein interaction and activation is well described. These residues are Gln181/194, Phe179/192, and Asn162/175<sup>23</sup>. Undoubtedly, the most crucial key residue observed in this study was Phe179/192, which was found to be important in the interaction of all ligands with both proteins. The Gln181/Gln194 was found to be important for RMT (both proteins) and 2-PMT (MT<sub>1</sub>) interaction, and Asn162/Asn175 was found to be important for RMT (both proteins) and 2-PMT (MT<sub>2</sub>). Hence, the importance of Gln181/Gln194 and Asn162/175 depends on binder and protein, which is not true for Phe179/192. In addition to these amino acids, three other conserve amino acids—Gly108/Gly121, Val111/Val124, and Val191/Val204—were shown to play important roles in the interaction with MT<sub>1</sub> and MT<sub>2</sub> for all binders. Beyond Gln181/194, Phe179/192, and Asn162/175 amino acids, only Thr178 and Met107 were recently observed in other studies involving binding with this protein<sup>73</sup>. Thus, we have potential amino acids crucial for protein–ligand interactions with both receptors. This could lead to more optimized molecule development based on the SBBD approach since key residues for the interaction of these molecules were identified, as well as the regions of the melatonin analogs that favored an increased affinity for the receptors. This is an important, although initial, step towards solving the issue of the short half-life of melatonin receptor ligands.

In conclusion, recent advances in deciphering the structures of MT<sub>1</sub> and MT<sub>2</sub> proteins have allowed for a detailed exploration of interactions with their binders. Molecular docking and dynamics simulations were employed to generate MT<sub>1</sub>-MLT and MT<sub>2</sub>-MLT complexes, revealing stronger binding to MT<sub>1</sub> than MT<sub>2</sub>. Notably, 2-PMT displayed higher affinity for both receptors compared to MLT, aligning with experimental findings. The analysis highlighted the importance of specific amino acids, such as Gln181/194, Phe179/192, and Asn162/175, in protein–ligand interactions, providing insights into potential therapeutic strategies. Also, it described new important interactions with Gly108/Gly121, Val111/Val124, and Val191/Val204.



This study enhances our understanding of receptor–ligand interactions and offers implications for future drug development. All the analyses of the interactions described here and the key regions of the receptors and ligands involved in the interactions are extremely relevant information for developing more effective drugs for treating sleep disorders. However, it is known that analyses involving drug optimization and mutation analysis are necessary to confirm the research data and fill these gaps. Future studies should consider the virtual screening of molecules with the important regions of the ligands (especially the aromatic rings) to find new ligands with greater affinity and optimize existing molecules by adding and/or removing groups that favor/disfavor interaction affinity.

## Methods

### Molecular docking and molecular dynamics simulation

Since there is no crystallized structure of the MT<sub>1</sub> and MT<sub>2</sub> proteins with MLT, the first step of the study involved obtaining the complexed structures through molecular docking using the AutoDock Vina program (referred to as Vina here)<sup>68</sup>. Initially, the three-dimensional (3D) structure of MLT was obtained from the PubChem website ([www.pubchem.ncbi.nlm.nih.gov/compound/896](http://www.pubchem.ncbi.nlm.nih.gov/compound/896)) in SDF format. The molecule's protonation at pH = 7.0 and 7.4 (following the protein experimental pH) was verified using the MarvinSketch code version 17.24 (Marvin Beans Suite – ChemAxon, [www.chemaxon.com](http://www.chemaxon.com)). Subsequently, the molecule was converted to PDBQT format using the OpenBabel<sup>74</sup> server.

The MT<sub>1</sub> structure was obtained from the Protein Data Bank ([www.rcsb.org](http://www.rcsb.org)). Four MT<sub>1</sub> crystals were compared for resolution, with codes 6ME2, 6ME3, 6ME4, and 6ME5. The crystal with the lowest resolution (6ME2<sup>25</sup>—2.8 Å), which suggests higher quality, was selected for MLT docking. The same procedure was followed for the MT<sub>2</sub> structure, where structures 6ME6, 6ME7, 6ME8, and 6ME9 were compared. The 6ME6<sup>23</sup> structure was chosen due to its lower resolution (2.8 Å) among MT<sub>2</sub> structures.

Before converting to the PDBQT format, the MT<sub>1</sub> and MT<sub>2</sub> proteins underwent a cleaning step, chain adjustments, and minimization on the Discovery Studios server. In this case, artifacts from the crystallization process were removed, as well as the ligands RMT and 2-PMT, bound to MT<sub>1</sub> and MT<sub>2</sub>, respectively. Additionally, missing side chains and hydrogen atoms were added. The protonations of the MT<sub>1</sub> and MT<sub>2</sub> proteins were evaluated on the online PropKa server for pH 7.0 and 7.4, respectively, in accordance with the crystallization experiment. After these modifications, the protein backbone's conformations were restrained, and an energy minimization (EM) step was performed using the CHARMM (Chemistry at Harvard Molecular Mechanics) force field. The EM utilized convergence tolerances of 10<sup>-5</sup> kcal/mol for total energy change, 10<sup>-3</sup> kcal/mol for the mean square root of the RMS gradient, and 10<sup>-5</sup> Å for the maximum atomic displacement, employing the Smart Minimizer algorithm. For the conversion of large molecules from PDB to PDBQT format, AutoDock Tools<sup>75</sup> was used.

The same binding sites of RMT and 2-PMT were considered for melatonin anchoring. For each system, the melatonin molecule was docked 1000 times, each time generating 10 binding conformation modes. The best conformation (lower Vina score) of each system was selected to proceed to MD simulations.

MD simulations were conducted to optimize the binder conformation within the binding pocket. Independent triplicate simulations were performed using GROMACS 2022 software<sup>81</sup>. The ligand parameters for the MD simulations were obtained using the ACPYPE server ([www.bio2byte.be/acpype/](http://www.bio2byte.be/acpype/))<sup>76</sup> with Gasteiger as the charge method and GAFF2 as the force field. The server provided all the necessary topology and parameter files for MD simulations using GROMACS software. The force field selected for protein was the Amberff99SB-ILDN. Six MD simulations were carried out for the protein–ligand complex, three for each MT<sub>1</sub> and MT<sub>2</sub> systems.

For each system, a cubic box was utilized with the TIP3P water model extended 12 Å away from solute atoms, and Cl<sup>-</sup> ions were added to neutralize it. Two rounds of energy minimization were executed to adjust unfavorable contacts in the initial structure. The first minimization step involves a maximum of 20000 steps or until the maximum force on any atom is reduced to below 50 kJ/mol/nm. The steepest descent algorithm was employed with protein restraint to focus on solvent relaxation. The second minimization step, without protein restraint, was performed in flexible water using the same steepest descent algorithm, and the maximum steps were increased to 10,000 or until the force on any atom fell below 250 kJ/mol/nm.

The system's pressure and temperature were adjusted to 1 atm and 310 K, in two separate 100 ps steps, referred to as the NVT ensemble (temperature setting) and NPT ensemble (pressure setting). The modified Berendsen<sup>77</sup> and Parrinello–Rahman<sup>78</sup> algorithms were applied to control the system temperature and pressure, respectively. Throughout both steps, hydrogen bonds were constrained using the LINCS algorithm<sup>79</sup>, and positional restraints were applied to the protein to stabilize the solvent around the solute.

Long-range electrostatic interactions were computed using the Particle Mesh Ewald (PME) summation method, employing a non-bonded interaction cut-off of 1 nm. The equations of motion were integrated using the leap-frog algorithm<sup>80</sup> with a time step of 0.2 fs. Before the MD simulation, a small NPT ensemble of 1 ns was conducted without any restrictions on protein position, followed by a production run for 200 ns without restrictions on protein conformation. The MD run produced a total of 2000 protein frames.

The gmx\_MMPBSA program<sup>81</sup> was employed to analyze the last 500 frames (50 ns) of the complexes for each MD simulation using hybrid Quantum Mechanics/Molecular Mechanics—Generalized-Born surface area (QM/MM-GBSA) free energy calculation. The QM region was limited to residues near 5 Å from the binder, and the applied semi-empirical functional was PM6-DH+. Solvent molecules and Cl<sup>-</sup> ions were excluded from the analysis. This method allowed the calculation of interaction energy for various conformations of the biological complex at a relatively low computational cost, enabling the selection of complexes with higher affinities for a more robust and accurate analysis using QM/DFT. Hence, the complexes with lower energy for each system were chosen for further QM (DFT) calculations using the MFCC approach.



The MD trajectories were visualized using UCSF Chimera software<sup>82</sup>. Root mean square deviation (RMSD) and fluctuation (RMSF) were calculated using the "gmx" commands of the GROMACS package. All plots were generated using the R language in RStudio 4.1.1 (<http://www.rstudio.com/>), and protein image representations were created using PyMol<sup>83</sup>.

### MFCC and quantum mechanical calculations

The QM calculation is an accurate methodology for studying ligand–protein interactions. However, it has been observed that the computational cost is significantly high for large systems. As the present study aims to analyze protein–ligand interactions, and therefore, is considered a complex biological system for QM calculations, the MFCC methodology developed by Zhang and Zhang<sup>71</sup> was applied to each of these systems to overcome this limitation. The MFCC scheme involves splitting the protein into individual amino acids by breaking the peptide bonds and calculating the interactions between each residue and the ligand separately. The summation of individual amino acid energies provides an approximate binding energy.

The MFCC approach employs "caps" to complete the valence of the amino acids after breaking the peptide bonds at both the N- and C-termini. These caps are composed of amino acid residues that precede and succeed the main amino acid. Additionally, the caps serve the purpose of closely reproducing the amino acid environment. Consequently, it becomes possible to calculate an approximate binding affinity for large systems, such as a protein–ligand complex.

Equation (1) presents the MFCC scheme for calculating the interaction energy (IE(BID/R<sup>i</sup>)) between the binder (BID) and the amino acid R<sup>i</sup>, with *i* denoting the *i*<sup>th</sup> amino acid of the protein chain.:

$$IE(BID/R^i) = E(BID + C^{i-1}R^iC^{i+1}) - E(C^{i-1}R^iC^{i+1}) - E(BID + C^{i-1}C^{i+1}) + E(C^{i-1}C^{i+1}) \quad (1)$$

The caps, represented as C<sup>*i*-1</sup> and C<sup>*i*+1</sup>, correspond to the neighboring residues covalently bonded to the amine and carboxyl groups of R<sup>*i*</sup>, respectively. The first term ( $E(BID + C^{i-1}R^iC^{i+1})$ ) calculates the interaction energy between the binder BID and the main residue (R<sup>*i*</sup>) bonded to the caps (C<sup>*i*-1</sup> and C<sup>*i*+1</sup>).

However, MFCC aims to assess the individual amino acid contributions to the binding affinity. Thus, the second and third terms are introduced to isolate the contribution of the main residue and eliminate the interaction energy between the binder and the caps. The second term ( $E(C^{i-1}R^iC^{i+1})$ ) represents the energy of the residue (R<sup>*i*</sup>) bonded to the caps (C<sup>*i*-1</sup> and C<sup>*i*+1</sup>), while the third term ( $E(BID + C^{i-1}C^{i+1})$ ) indicates the interaction energy between the BID and the caps (C<sup>*i*-1</sup> and C<sup>*i*+1</sup>). Subtracting the energies calculated in the second and third terms from the first term removes their influence on the energy interaction between BID and R<sup>*i*</sup>.

Since the caps' energies were subtracted twice (in the second and third terms), it becomes necessary to add them back in the fourth term ( $E(C^{i-1}C^{i+1})$ ) to account for their effect on the energy interaction between BID and R<sup>*i*</sup>. This step accurately evaluates the individual amino acid's contribution to the overall binding affinity.

For the MFCC involving the MLT molecule, the frames with the lowest energy obtained from the QM/MM-GBSA analysis of MT<sub>1</sub> and MT<sub>2</sub> were selected. No modification was needed since the structures were adjusted previously. As for the 2-PMT molecule, the structures were obtained from the PDB, where the structures of MT<sub>1</sub> and MT<sub>2</sub> were submitted under accession codes 6ME3<sup>25</sup> and 6ME6<sup>23</sup>, respectively. The crystallographic structures of the MT<sub>1</sub>-RMT and MT<sub>2</sub>-RMT complexes were taken from the PDB (PDB codes: 6ME2<sup>25</sup> and 6ME9<sup>23</sup>, respectively). As mentioned earlier, structural adjustments are necessary to address potential limitations of the X-ray technique. Thus, the same cleaning procedure, protonation verification at pH 7.0 (MT<sub>1</sub>) and 7.4 (MT<sub>2</sub>) (for both ligands and receptors), the addition of missing side chains, and energy minimization, as performed previously, were applied to these structures. The only difference is that the 2-PMT and MLT molecules were retained in the structures.

After performing fragmentation for each amino acid, the interaction energy between the receptor and the binder was computed using the Gaussian 16 package<sup>84</sup>, which employs the density functional theory (DFT) formalism<sup>85,86</sup>. The simulations were carried out using the generalized gradient approximation (GGA) with the B97D functional, which has been proven to be an efficient and accurate QM method for large systems, particularly when dispersion forces play a significant role<sup>87</sup>. To represent the Kohn–Sham orbitals for all electrons, a small basis set 6-311+G(d,p) with triple split valence (valence triple-zeta), an additional diffuse function (+), and polarization functions (d,p) were applied. The conductor-like polarizable continuum model (CPCM) was utilized to account for solvent effects in the QM calculations, using dielectric constants ( $\epsilon$ ) of 10 and 40. The constant of 40 is reported as being similar to the crystalline environment<sup>57,58,88</sup>. Meanwhile, the constant of 10 is used here as a control, where a lower constant is expected to result in a higher medium permittivity and lower energy values. Thus, we can ensure that calculations for both constants were performed correctly. Each term of Equation (1) was obtained from the DFT simulations.

It has been established that as the amino acids are increasingly distant from the binder, their contribution to the binding energy with the small molecule is reduced. To eliminate the calculation of unimportant interactions, a convergence analysis of the total binding energy was conducted to limit the number of amino acid residues considered. The analysis incorporated the closest residues from the binding site and excluded the most distant ones. The interaction energy of amino acid residues within imaginary spheres with a pocket radius of *r* centered at the binder was evaluated, where  $r = R/2$  (for  $R = 1, 2, 3, 4, \dots, N_n$ ; with  $N_n$  being the next natural number of sequences)<sup>88</sup>. The convergence criteria were met when the total energy, while increasing the radius *r*, did not change by more than 10% compared to the previous radius value.

## Alanine scanning

To verify the significance of amino acids in protein–ligand interactions, the PremPLI server was utilized to conduct an alanine scanning study, wherein the original amino acid was substituted with alanine. This server employs machine learning through a random forest algorithm, with training data based on experimental data from 796 mutations across 360 protein–ligand complexes<sup>89</sup>.

Consequently, the server can predict the effect on protein–ligand interaction using  $\Delta\Delta G$ , where positive values correspond to decreased interaction and negative values indicate increased interaction.

In the present study, the analysis focused on the amino acids Gly108/Gly121, Val111/Val124, and Val191/Val204 for all ligands. The analysis of amino acids Gln181/194, Phe179/192, and Asn162/175 was limited to those ligands that exhibited strong interaction.

## Data availability

The datasets analyzed during the current study are available in the Protein Data Bank repository, following the web links: <https://www.rcsb.org/structure/6ME2>, <https://www.rcsb.org/structure/6ME3>, <https://www.rcsb.org/structure/6ME6>, <https://www.rcsb.org/structure/6ME9>, <https://www.rcsb.org/structure/7VH0> and <https://www.rcsb.org/structure/7DB6>. Additional datasets used and/or analyzed during the current study are available from the corresponding author upon reasonable request.

Received: 8 February 2024; Accepted: 15 April 2024

Published online: 13 May 2024

## References

- Lerner, A. B., Case, J. D., Takahashi, Y., Lee, T. H. & Mori, W. Isolation of melatonin, the pineal gland factor that lightens melano-cytes. *J. Am. Chem. Soc.* **80**, 2587–2587. <https://doi.org/10.1021/ja01543a060> (1958).
- Pandi-Perumal, S. R. *et al.* Physiological effects of melatonin: Role of melatonin receptors and signal transduction pathways. *Prog. Neurobiol.* **85**, 335–353. <https://doi.org/10.1016/j.pneurobio.2008.04.001> (2008).
- Reiter, R. J. The melatonin rhythm: Both a clock and a calendar. *Experientia* **49**, 654–664. <https://doi.org/10.1007/bf01923947> (1993).
- Ishida, N., Kaneko, M. & Allada, R. Biological clocks. *Proc. Natl. Acad. Sci.* **96**, 8819–8820. <https://doi.org/10.1073/pnas.96.16.8819> (1999).
- Hattar, S., Liao, H.-W., Takao, M., Berson, D. M. & Yau, K.-W. Melanopsin-containing retinal ganglion cells: Architecture, projections, and intrinsic photosensitivity. *Science* **295**, 1065–1070 (2002).
- Cardinali, D. P. & Pévet, P. Basic aspects of melatonin action. *Sleep Med. Rev.* **2**, 175–190 (1998).
- Cardinali, D. & Rosner, J. Metabolism of serotonin by the rat retina in vitro. *J. Neurochem.* **18**, 1769–1770 (1971).
- Cardinali, D. P., Larin, F. & Wurtman, R. J. Action spectra for effects of light on hydroxyindole-o-methyl transferases in rat pineal, retina and harderian gland. *Endocrinology* **91**, 877–886 (1972).
- Tosini, G. & Menaker, M. The clock in the mouse retina: Melatonin synthesis and photoreceptor degeneration. *Brain Res.* **789**, 221–228 (1998).
- Raikhlin, N. T. & Kvetnoy, I. M. Melatonin and enterochromaffine cells. *Acta Histochem.* **55**, 19–24 (1976).
- Slominski, A. *et al.* On the role of melatonin in skin physiology and pathology. *Endocrine* **27**, 137–147 (2005).
- Carrillo-Vico, A. *et al.* Evidence of melatonin synthesis by human lymphocytes and its physiological significance: Possible role as intracrine, autocrine, and/or paracrine substance. *FASEB J.* **18**, 537–539 (2004).
- Conti, A. *et al.* Evidence for melatonin synthesis in mouse and human bone marrow cells. *J. Pineal Res.* **28**, 193–202 (2000).
- Reppert, S. M., Weaver, D. R. & Ebisawa, T. Cloning and characterization of a mammalian melatonin receptor that mediates reproductive and circadian responses. *Neuron* **13**, 1177–1185 (1994).
- Reppert, S. M. *et al.* Molecular characterization of a second melatonin receptor expressed in human retina and brain: The mel1b melatonin receptor. *Proc. Natl. Acad. Sci.* **92**, 8734–8738 (1995).
- Dubocovich, M. L. & Markowska, M. Functional mt1 and mt2 melatonin receptors in mammals. *Endocrine* **27**, 101–110 (2005).
- Liu, C. *et al.* Molecular dissection of two distinct actions of melatonin on the suprachiasmatic circadian clock. *Neuron* **19**, 91–102 (1997).
- Al-Ghoul, W. M., Herman, M. D. & Dubocovich, M. L. Melatonin receptor subtype expression in human cerebellum. *Neuroreport* **9**, 4063–4068 (1998).
- Clemens, J., Jarzynka, M. & Witt-Enderby, P. Down-regulation of mt1 melatonin receptors in rat ovary following estrogen exposure. *Life Sci.* **69**, 27–35 (2001).
- Frungeri, M. B. *et al.* Direct effect of melatonin on syrian hamster testes: melatonin subtype 1a receptors, inhibition of androgen production, and interaction with the local corticotropin-releasing hormone system. *Endocrinology* **146**, 1541–1552 (2005).
- Naji, L., Carrillo-Vico, A., Guerrero, J. M. & Calvo, J. R. Expression of membrane and nuclear melatonin receptors in mouse peripheral organs. *Life Sci.* **74**, 2227–2236 (2004).
- Hardeland, R., Pandi-Perumal, S. & Cardinali, D. P. Melatonin. *Int. J. Biochem. Cell Biol.* **38**, 313–316. <https://doi.org/10.1016/j.biocel.2005.08.020> (2006).
- White, K. L. *et al.* Structural connection between activation microswitch and allosteric sodium site in gpcr signaling. *Structure* **26**, 259–269 (2018).
- Johansson, L. C. *et al.* XFEL structures of the human MT<sub>2</sub> melatonin receptor reveal the basis of subtype selectivity. *Nature* **569**, 289–292. <https://doi.org/10.1038/s41586-019-1144-0> (2019).
- Stauch, B. *et al.* Structural basis of ligand recognition at the human MT<sub>1</sub> melatonin receptor. *Nature* **569**, 284–288. <https://doi.org/10.1038/s41586-019-1141-3> (2019).
- Riemann, D., Krone, L. B., Wulff, K. & Nissen, C. Sleep, insomnia, and depression. *Neuropsychopharmacology* **45**, 74–89. <https://doi.org/10.1038/s41386-019-0411-y> (2019).
- Ozminkowski, R. J., Wang, S. & Walsh, J. K. The direct and indirect costs of untreated insomnia in adults in the United States. *Sleep* **30**, 263–273. <https://doi.org/10.1093/sleep/30.3.263> (2007).
- Wardle-Pinkston, S., Slavish, D. C. & Taylor, D. J. Insomnia and cognitive performance: A systematic review and meta-analysis. *Sleep Med. Rev.* **48**, 101205. <https://doi.org/10.1016/j.smrv.2019.07.008> (2019).
- Johnson, K. A. *et al.* The association of insomnia disorder characterised by objective short sleep duration with hypertension, diabetes and body mass index: A systematic review and meta-analysis. *Sleep Med. Rev.* **59**, 101456. <https://doi.org/10.1016/j.smrv.2021.101456> (2021).

30. Shan, Z. *et al.* Sleep duration and risk of type 2 diabetes: A meta-analysis of prospective studies. *Diabetes Care* **38**, 529–537. <https://doi.org/10.2337/dc14-2073> (2015).
31. Jarrin, D. C. *et al.* Insomnia and hypertension: A systematic review. *Sleep Med. Rev.* **41**, 3–38. <https://doi.org/10.1016/j.smrv.2018.02.003> (2018).
32. Montgomery, P. A systematic review of non-pharmacological therapies for sleep problems in later life. *Sleep Med. Rev.* **8**, 47–62. [https://doi.org/10.1016/s1087-0792\(03\)00026-1](https://doi.org/10.1016/s1087-0792(03)00026-1) (2004).
33. Morin, C. M. *et al.* Nonpharmacologic treatment of chronic insomnia. *Sleep* **22**, 1134–1156. <https://doi.org/10.1093/sleep/22.8.1134> (1999).
34. Morin, A. K. Strategies for treating chronic insomnia. *Am. J. Managed Care* **12**, S230–S245 (2006).
35. Nowell, P. D. *et al.* Benzodiazepines and zolpidem for chronic insomnia: A meta-analysis of treatment efficacy. *JAMA* **278**, 2170–2177 (1997).
36. Srinivasan, V. *et al.* Melatonin agonists in primary insomnia and depression-associated insomnia: Are they superior to sedative-hypnotics?. *Prog. Neuro-Psychopharmacol. Biol. Psychiatry* **35**, 913–923. <https://doi.org/10.1016/j.pnpbp.2011.03.013> (2011).
37. Victorri-Vigneau, C., Dailly, E., Veyrac, G. & Jolliet, P. Evidence of zolpidem abuse and dependence: results of the French centre for evaluation and information on pharmacodependence (ceip) network survey. *Br. J. Clin. Pharmacol.* **64**, 198–209 (2007).
38. Black, L. I., Clarke, T. C., Barnes, P. M., Stussman, B. J. & Nahin, R. L. Use of complementary health approaches among children aged 4–17 years in the United States: National health interview survey, 2007–2012. *Natl. Health Stat. Rep.* **1** (2015).
39. Auger, R. R. *et al.* Clinical practice guideline for the treatment of intrinsic circadian rhythm sleep-wake disorders: advanced sleep-wake phase disorder (aswpd), delayed sleep-wake phase disorder (dswpd), non-24-hour sleep-wake rhythm disorder (n24swd), and irregular sleep-wake rhythm disorder (iswrtd). an update for 2015: an american academy of sleep medicine clinical practice guideline. *J. Clin. Sleep Med.* **11**, 1199 (2015).
40. DeMuro, R. L., Nafziger, A. N., Blask, D. E., Menhinick, A. M. & Bertino, J. S. Jr. The absolute bioavailability of oral melatonin. *J. Clin. Pharmacol.* **40**, 781–784 (2000).
41. Grigg-Damberger, M. M. & Ianakieva, D. Poor quality control of over-the-counter melatonin: What they say is often not what you get. *J. Clin. Sleep Med.* **13**, 163–165. <https://doi.org/10.5664/jcsm.6434> (2017).
42. Wade, A. G. *et al.* Efficacy of prolonged release melatonin in insomnia patients aged 55–80 years: quality of sleep and next-day alertness outcomes. *Curr. Med. Res. Opin.* **23**, 2597–2605. <https://doi.org/10.1185/030079907x233098> (2007).
43. Duranti, E. *et al.* 2-bromomelatonin: Synthesis and characterization of a potent melatonin agonist. *Life Sci.* **51**, 479–485. [https://doi.org/10.1016/0024-3205\(92\)90024-j](https://doi.org/10.1016/0024-3205(92)90024-j) (1992).
44. Chen, J. J., Fiehn-Schulze, B., Brough, P. A., Snieckus, V. & Firnau, G. Synthesis of 2-iodo- and 2-phenyl-[11c]melatonin: Potential PET tracers for melatonin binding sites. *Appl. Radiat. Isot.* **49**, 1573–1579. [https://doi.org/10.1016/s0969-8043\(98\)00005-0](https://doi.org/10.1016/s0969-8043(98)00005-0) (1998).
45. Spadoni, G. *et al.* 2-substituted 5-methoxy-n-acyltryptamines: synthesis, binding affinity for the melatonin receptor, and evaluation of the biological activity. *J. Med. Chem.* **36**, 4069–4074. <https://doi.org/10.1021/jm00077a010> (1993).
46. Cajoche, C. Tak-375 takeda. *Current opinion investigational drugs (London, Engl. : 2000)* **6**, 114–121 (2005).
47. Miyamoto, M. Pharmacology of ramelteon, a selective MTsub1/sub2/subreceptor agonist: A novel therapeutic drug for sleep disorders. *CNS Neurosci. & Ther.* **15**, 32–51. <https://doi.org/10.1111/j.1755-5949.2008.00066.x> (2009).
48. Erman, M., Seiden, D. & Zammit, G. Phase ii study of the selective ml-1 receptor agonist tak-375 in subjects with primary chronic insomnia. In *Sleep*, vol. 26, A298–A298 (AMER ACADEMY SLEEP MEDICINE ONE WESTBROOK CORPORATE CENTER STE 920, 2003).
49. Karim, A., Tolbert, D. & Cao, C. Disposition kinetics and tolerance of escalating single doses of ramelteon, a high-affinity MTsub1/suband MTsub2/submelatonin receptor agonist indicated for treatment of insomnia. *J. Clin. Pharmacol.* **46**, 140–148. <https://doi.org/10.1177/0091270005283461> (2006).
50. Stevenson, S. Study of the absorption, metabolism, and excretion of (14c)-ramelteon (TAK-375). *Clin. Pharmacol. Ther.* **75**, P22. <https://doi.org/10.1016/j.clpt.2003.11.084> (2004).
51. Takeda pharmaceuticals america inc. rozerem™ (ramelteon) tablets: prescribing information [online]. <https://www.general.takedapharm.com/rozerempi/>. Accessed: 2023–01–22.
52. Roth, T. *et al.* Phase iii outpatient trial of ramelteon for the treatment of chronic insomnia in elderly patients. In *Journal of the American Geriatrics Society*, vol. 53, S25–S25 (WILEY-BLACKWELL 111 RIVER ST, HOBOKEN 07030–5774, NJ USA, 2005).
53. Zammit, G., Roth, T., Erman, M. *et al.* Polysomnography and outpatient study to determine the efficacy of ramelteon in adults with chronic insomnia [abstract no. nr613 plus poster]. In *158th Annual Meeting of the American Psychiatric Association: New Research Abstracts*, 21–26 (2005).
54. Zammit, G. *et al.* Phase iii study of ramelteon in a first-night-effect model of transient insomnia. *Sleep Med* **6**, S50–S51 (2005).
55. McGechan, A. & Wellington, K. Ramelteon. *CNS Drugs* **19**, 1057–1065 (2005).
56. Elisi, G. M. *et al.* In silico drug discovery of melatonin receptor ligands with therapeutic potential. *Expert. Opin. Drug Discov.* **17**, 343–354. <https://doi.org/10.1080/17460441.2022.2043846> (2022).
57. Stein, R. M. *et al.* Virtual discovery of melatonin receptor ligands to modulate circadian rhythms. *Nature* **579**, 609–614. <https://doi.org/10.1038/s41586-020-2027-0> (2020).
58. Glatfelter, G. *et al.* In vivo/i efficacy of novel type preferring MT sub1/sub melatonin receptor inverse agonists in c3h/HeN mouse models of chronobiological behavior. *FASEB J.* **34**, 1–1. <https://doi.org/10.1096/fasebj.2020.34.s1.04127> (2020).
59. Campos, D. M. O. *et al.* Intermolecular interactions of cn-716 and acyl-KR-aldehyde dipeptide inhibitors against Zika virus. *Phys. Chem. Chem. Phys.* **22**, 15683–15695. <https://doi.org/10.1039/d0cp02254c> (2020).
60. Bezerra, K. S. *et al.* Ribosomal RNA–aminoglycoside hygromycin b interaction energy calculation within a density functional theory framework. *J. Phys. Chem. B* **123**, 6421–6429. <https://doi.org/10.1021/acs.jpcc.9b04468> (2019).
61. Vianna, J. F., Bezerra, K. S., Oliveira, J. I. N., Albuquerque, E. L. & Fulco, U. L. Binding energies of the drugs capreomycin and streptomycin in complex with tuberculosis bacterial ribosome subunits. *Phys. Chem. Chem. Phys.* **21**, 19192–19200. <https://doi.org/10.1039/c9cp03631h> (2019).
62. Neto, J. X. L. *et al.* Exploring the binding mechanism of GABAsubb/sub receptor agonists and antagonists through in silico simulations. *J. Chem. Inf. Model.* **60**, 1005–1018. <https://doi.org/10.1021/acs.jcim.9b01025> (2019).
63. Nyambo, K. *et al.* Molecular docking, molecular dynamics simulations and binding free energy studies of interactions between mycobacterium tuberculosis pks13, pkng and bioactive constituents of extremophilic bacteria. *Sci. Rep.* <https://doi.org/10.1038/s41598-024-57124-9> (2024).
64. He, Y. *et al.* Using deep learning and molecular dynamics simulations to unravel the regulation mechanism of peptides as non-competitive inhibitor of xanthine oxidase. *Sci. Rep.* <https://doi.org/10.1038/s41598-023-50686-0> (2024).
65. Dewar, M. J. S., Zoebisch, E. G., Healy, E. F. & Stewart, J. J. P. Development and use of quantum mechanical molecular models. 76. AM1: A new general purpose quantum mechanical molecular model. *J. Am. Chem. Soc.* **107**, 3902–3909. <https://doi.org/10.1021/ja00299a024> (1985).
66. Stewart, J. J. P. Optimization of parameters for semiempirical methods i. method. *J. Comput. Chem.* **10**, 209–220. <https://doi.org/10.1002/jcc.540100208> (1989).
67. Sanachai, K. *et al.* Insights into the binding recognition and susceptibility of tofacitinib toward janus kinases. *ACS Omega* **5**, 369–377. <https://doi.org/10.1021/acsomega.9b02800> (2020).

68. Kar, R. K. Benefits of hybrid qm/mm over traditional classical mechanics in pharmaceutical systems. *Drug Discov. Today* **28**, 103374. <https://doi.org/10.1016/j.drudis.2022.103374> (2023).
69. Kohn, W. & Sham, L. J. Self-consistent equations including exchange and correlation effects. *Phys. Rev.* **140**, A1133–A1138. <https://doi.org/10.1103/physrev.140.a1133> (1965).
70. Albuquerque, E., Fulco, U. L., Caetano, E. & Freire, V. *Quantum Chemistry Simulation of Biological Molecules* (Cambridge University Press, 2020).
71. Zhang, D. W. & Zhang, J. Molecular fractionation with conjugate caps for full quantum mechanical calculation of protein–molecule interaction energy. *J. Chem. Phys.* **119**, 3599–3605 (2003).
72. Trott, O. & Olson, A. J. AutoDock vina: Improving the speed and accuracy of docking with a new scoring function, efficient optimization, and multithreading. *J. Comput. Chem.* <https://doi.org/10.1002/jcc.21334> (2009).
73. Okamoto, H. H. *et al.* Cryo-EM structure of the human mt1-gi signaling complex. *Nat. Struct. & Mol. Biol.* **28**, 694–701. <https://doi.org/10.1038/s41594-021-00634-1> (2021).
74. Wang, Q. *et al.* Structural basis of the ligand binding and signaling mechanism of melatonin receptors. *Nat. Commun.* <https://doi.org/10.1038/s41467-022-28111-3> (2022).
75. Özçelik, R., van Tilborg, D., Jiménez-Luna, J. & Grisoni, F. Structure-based drug discovery with deep learning\*\*. *ChemBioChem* <https://doi.org/10.1002/cbic.202200776> (2023).
76. Nosjean, O. *et al.* Comparative pharmacological studies of melatonin receptors: Mt1, mt2 and mt3/qr2. *Biochem. Pharmacol.* **61**, 1369–1379. [https://doi.org/10.1016/s0006-2952\(01\)00615-3](https://doi.org/10.1016/s0006-2952(01)00615-3) (2001).
77. Kato, K. *et al.* Neurochemical properties of ramelteon (TAK-375), a selective mt1/mt2 receptor agonist. *Neuropharmacology* **48**, 301–310. <https://doi.org/10.1016/j.neuropharm.2004.09.007> (2005).
78. Miyamoto, M. Pharmacology of ramelteon, a selective mt1/mt2 receptor agonist: A novel therapeutic drug for sleep disorders. *CNS Neurosci. Ther.* **15**, 32–51. <https://doi.org/10.1111/j.1755-5949.2008.00066.x> (2009).
79. O’Boyle, N. M. *et al.* Open babel: An open chemical toolbox. *J. Cheminformatics* <https://doi.org/10.1186/1758-2946-3-33> (2011).
80. Huey, R., Morris, G. M. & Forli, S. Using autodock 4 and autodock vina with autodocktools: a tutorial. *The Scripps Res. Inst. Mol. Graph. Lab.* **10550**, 1000 (2012).
81. Spoel, D. V. D. *et al.* GROMACS: Fast, flexible, and free. *J. Comput. Chem.* **26**, 1701–1718. <https://doi.org/10.1002/jcc.20291> (2005).
82. da Silva, A. W. S. & Vranken, W. F. ACPYPE - AnteChamber PYthon parser interface. *BMC Res. Notes* <https://doi.org/10.1186/1756-0500-5-367> (2012).
83. Berendsen, H. J. C., Postma, J. P. M., van Gunsteren, W. F., DiNola, A. & Haak, J. R. Molecular dynamics with coupling to an external bath. *J. Chem. Phys.* **81**, 3684–3690. <https://doi.org/10.1063/1.448118> (1984).
84. Hutter, J. Car-parrinello molecular dynamics. *Wiley Interdiscip. Rev. Comput. Mol. Sci.* **2**, 604–612. <https://doi.org/10.1002/wcms.90> (2011).
85. Hess, B., Bekker, H., Berendsen, H. J. C. & Fraaije, J. G. E. M. LINCS: A linear constraint solver for molecular simulations. *J. Comput. Chem.* **18**, 1463–1472. [https://doi.org/10.1002/\(sici\)1096-987x\(199709\)18:12<1463::aid-jcc4>3.0.co;2-h](https://doi.org/10.1002/(sici)1096-987x(199709)18:12<1463::aid-jcc4>3.0.co;2-h) (1997).
86. Hockney, R., Goel, S. & Eastwood, J. Quiet high-resolution computer models of a plasma. *J. Comput. Phys.* **14**, 148–158. [https://doi.org/10.1016/0021-9991\(74\)90010-2](https://doi.org/10.1016/0021-9991(74)90010-2) (1974).
87. Valdés-Tresanco, M. S., Valdés-Tresanco, M. E., Valiente, P. A. & Moreno, E. gmx\_MMPBSA: A new tool to perform end- state free energy calculations with GROMACS. *J. Chem. Theory Comput.* **17**, 6281–6291. <https://doi.org/10.1021/acs.jctc.1c00645> (2021).
88. Pettersen, E. F. *et al.* UCSF chimera: A visualization system for exploratory research and analysis. *J. Comput. Chem.* **25**, 1605–1612. <https://doi.org/10.1002/jcc.20084> (2004).
89. DeLano, W. L. *et al.* Pymol: An open-source molecular graphics tool. *CCP4 Newsl. Protein Crystallogr* **40**, 82–92 (2002).
90. Frisch, M. e. *et al.* Gaussian 16 (2016).
91. Adamo, C., Cossi, M., Rega, N. & Barone, V. New computational strategies for the quantum mechanical study of biological systems in condensed phases. In *Theoretical and Computational Chemistry*, vol. 9, 467–538 (Elsevier, 2001).
92. Car, R. Introduction to density-functional theory and ab-initio molecular dynamics. *Quant. Struct. Relationships* **21**, 97–104 (2002).
93. Albuquerque, E. L. *et al.* Dna-based nanobiostructured devices: The role of quasiperiodicity and correlation effects. *Phys. Rep.* **535**, 139–209 (2014).
94. Grimme, S. Semiempirical gga-type density functional constructed with a long-range dispersion correction. *J. Comput. Chem.* **27**, 1787–1799 (2006).
95. Vianna, J. *et al.* New ethionamide boosters and ethr2: structural and energetic analysis. *Phys. Chem. Chem. Phys.* **23**, 23233–23241 (2021).
96. Sun, T., Chen, Y., Wen, Y., Zhu, Z. & Li, M. Prempli: a machine learning model for predicting the effects of missense mutations on protein-ligand interactions. *Commun. Biol.* <https://doi.org/10.1038/s42003-021-02826-3> (2021).

## Acknowledgements

This work was partially financed by the Brazilian Research Agencies CAPES and CNPq. We would like to thank the Núcleo de Processamento de Alto Desempenho (NPAD) of the Universidade Federal do Rio Grande do Norte for allowing us to use their computer facilities. DSG acknowledges the Center for Computational Engineering Sciences (CCES) at Unicamp for financial support through the FAPESP/CEPID Grant 2013/08293-7.

## Author contributions

G.L.M: conceptualization, data curation; formal analysis; investigation; visualization; writing—original draft preparation. K.S.B: data curation; methodology; project administration; supervision; writing—review & editing. J.I.N.O: conceptualization; data curation; methodology; project administration; resources; supervision; writing—review & editing. J.F.A.: conceptualization; writing—original draft. D.S.G: supervision; writing—review & editing. R.A.S: visualization, writing—review & editing. M.V.S: investigation, writing—review & editing. U.L.F: conceptualization; data curation; methodology; project administration; resources; supervision; writing—review & editing.

## Competing interests

The authors declare no competing interests.

## Additional information

**Supplementary Information** The online version contains supplementary material available at <https://doi.org/10.1038/s41598-024-59786-x>.

**Correspondence** and requests for materials should be addressed to U.L.F.



**Reprints and permissions information** is available at [www.nature.com/reprints](http://www.nature.com/reprints).

**Publisher's note** Springer Nature remains neutral with regard to jurisdictional claims in published maps and institutional affiliations.



**Open Access** This article is licensed under a Creative Commons Attribution 4.0 International License, which permits use, sharing, adaptation, distribution and reproduction in any medium or format, as long as you give appropriate credit to the original author(s) and the source, provide a link to the Creative Commons licence, and indicate if changes were made. The images or other third party material in this article are included in the article's Creative Commons licence, unless indicated otherwise in a credit line to the material. If material is not included in the article's Creative Commons licence and your intended use is not permitted by statutory regulation or exceeds the permitted use, you will need to obtain permission directly from the copyright holder. To view a copy of this licence, visit <http://creativecommons.org/licenses/by/4.0/>.

© The Author(s) 2024